Design, Fabrication and Preliminary Testing of a Composite Reinforced Timber Guardrail

Dr. William G. Davids, PI
Joshua K. Botting, Graduate Research Assistant

Prepared for
The New England Transportation Consortium

March 31, 2004
NETCR39 **Project No. 00-3**

Technical Report Documentation Page

1. Report No.	2. Government Accession No.	3. Recepient's Catalog No.
NETCR39	N/A	N/A

4. Title and Subtitle	5. Report Date
Design, Fabrication and Preliminary Testing of a Composite Reinforced Timber Guardrail	Mar. 31, 2004
	6. Performing Organization Code: N/A

7. Author(s)	8. Performing Organization Report No.
Dr. William G. Davids, PI Joshua K. Botting	N/A

9. Performing Organization Name and Address	10 Work Unit No. (TRAIS)
Department of Civil and Environmental Engineering University of Maine 5711 Boardman Hall Orono, ME 04469-5711	N/A
	11. Contract or Grant No.: N/A
12. Sponsoring Agency Name and Address New England Transportation Consortium 179 Middle Turnpike University of Connecticut, U-202 Storrs, CT 06269-5202	13. Type of Report and Period Covered Final Report 7/01 – 12/03
	14. Sponsoring Agency Code NETC 00-3 A Study Conducted in Cooperation with the US DOT

15 Supplementary Notes
N/A

16. Abstract

An FRP-reinforced hardwood glulam guardrail was designed and tested for durability and the potential to pass a TL-3 vehicular crash test. The research conducted in this study combined dynamic structural analysis of the guardrail system under vehicular impact with a carefully designed laboratory testing program to establish the adequacy of the guardrail. The results of this research indicate that the guardrail as designed and tested is structurally adequate, and when preservative treated, should be sufficiently durable for exterior use. A unique bolted steel splice connection was developed to transfer tensile forces between 3.65m-long rail sections. This splice is critical to the crashworthiness of the rail, and allows easy installation and replacement of damaged rail sections. The rail section is lighter and easier to install than existing timber guardrail alternatives, and is expected to be cost-competitive for applications where an aesthetically pleasing timber guardrail is required.

17. Key Words	18. Distribution Statement
glulam, FRP composites, structural testing, timber connections, bolted connections, guardrail impact	No restrictions. This document is available to the public through the National Technical Information Service, Springfield, Virginia 22161.

19. Security Classif. (of this report)	20. Security Classif. (of this page)	21. No. of Pages	21. Price
Unclassified	Unclassified	63	N/A

Form DOT F 1700.7 (8-72) Reproduction of completed page authorized

METRIC CONVERSION PAGE

Metric Unit	Equivalent English Unit
1 mm	0.0394 in
1 m	3.281 ft
1 N	0.225 lbs
1 kN	224.7 lbs
1 MN	224700 lbs
1 kg	2.205 lb-m
1 L	0.264 gal

TABLE OF CONTENTS

Technical Report Documentation Page ii
Metric Conversion Page iii
List of Tables vi
List of Figures vii
1. Introduction 1
1.1. Background 1
1.2. Guardrail Overview 1
1.3. Report Organization 2
2. Guardrail Modeling 2
2.1. Overview 2
2.2. Guardrail Performance Limits 3
2.3. Guardrail System Model 4
2.4. Element Length Convergence Study 5
2.5. Time Step Convergence Study 7
2.6. Guardrail System Analysis Results 8
2.7. Conclusions 9
3. Guardrail Section Design, Fabrication, And Durability Testing 10
3.1. Reinforced Cross-Section Design 10
3.1.1 Sizing of Guardrail 10
3.1.2 Material Selection 10
3.1.3 Lamination Scheme 11
3.1.4 Brickwork Lamination Design 12
3.2. Reinforced Glulam Fabrication 12
3.2.1 Glulam Layup 12
3.2.2 Bonding FRP to the Glulam Rail 14
3.3. Durability Testing 14
3.4. Cost Analysis 15
4. Flexural Testing 17
4.1. Test Setup 17
4.2. Instrumentation 18
4.3. Test Results 18
4.4. Determination of the Elastic Modulus and Effective Section Properties 21
4.5. Summary 21

TABLE OF CONTENTS (con't)

5. Design and Testing of Field Splice Connection 22
   5.1. Overview of Splice Connection 22
   5.2. Fabrication of Splice Connection Specimens 24
   5.3. Connection Testing Program 25
      5.3.1 Tension Test Setup....25
      5.3.2 Instrumentation 26
   5.4. Test Results 26
      5.4.1 Results for 126 N-m of Initial Bolt Torque....26
      5.4.2 Results for 54 N-m of Initial Bolt Torque....30
      5.4.3 Results for 27 N-m of Initial Bolt Torque....32
   5.5. Durability Testing 35
   5.6. Summary 37
6. Combined Bending and Tension Testing 37
   6.1. Design of Bending-Tension Reaction Fixture 37
   6.2. Bending-Tension Test Setup 40
      6.2.1 Fabrication of Combined Bending and Tension Specimens....40
      6.2.2 Combined Bending and Tension Test Setup....41
      6.2.3 Instrumentation and Data Acquisition 42
   6.3. Bending-Tension Test Results 42
      6.3.1 Specimen BT1....42
      6.3.2 Specimen BT2....45
      6.3.3 Specimen BT3....47
   6.4. Summary and Conclusions....49
7. Summary and Conclusions 50
   7.1. Summary 50
   7.2. Conclusions and Recommendations 51
8. References....53
9. Appendix....55

LIST OF TABLES

Table 2.1 Cross-Section Properties Used in Analyses 9
Table 2.2 Cross-Section Properties Used in Analyses 9
Table 3.1 Guardrail Cost Estimate 16
Table 6.1 Summary of Bending-Tension Test Results 49

LIST OF FIGURES

Figure 1.1 Glulam Guardail Cross-Section....2
Figure 2.1 Guardrail System Layout....5
Figure 2.2 Displacement Convergence with Decreasing Element Size....6
Figure 2.3 Convergence of Impact Duration with Decreasing Element Size....7
Figure 2.4 Convergence of Axial Force with Decreasing Time Step....8
Figure 2.5 Maximum Axial Force in the Rail Splice Connection....9
Figure 3.1 Glulam Brickwork Layup....12
Figure 3.2 Resin Application and Lamination Stacking....13
Figure 4.1 Flexural Test Setup....17
Figure 4.2 Strain Gage Locations....18
Figure 4.3 Flexural Load-Displacement Response....18
Figure 4.4 Compressive Response of Load Head and Rubber Pad....19
Figure 4.5 Load-Strain Response....20
Figure 4.6 Flexural Failure Modes....20
Figure 5.1 Splice Connection....23
Figure 5.2 Typical Tension Specimen....26
Figure 5.3 Load-Strain Relation for Specimen T1....27
Figure 5.4 Load vs. Crosshead Position for Specimen T1....28
Figure 5.5 Bolt Plug Tear-Out for Specimen T1....28
Figure 5.6 Load-Strain Relation for Specimen T2....29
Figure 5.7 Load vs. Crosshead Position for Specimen T2....29
Figure 5.8 Load-Strain Relation for Specimen T3....30
Figure 5.9 Load vs. Crosshead Position for Specimen T3....31
Figure 5.10 Load-Strain Relation for Specimen T4....31
Figure 5.11 Load vs. Crosshead Position for Specimen T4....32
Figure 5.12 Load-Strain Relation for Specimen T5....33
Figure 5.13 Load vs. Crosshead Position for Specimen T5....33
Figure 5.14 Load-Strain Relation for Specimen T6....34
Figure 5.15 Load vs. Crosshead Position for Specimen T6....34
Figure 5.16 ASTM D1101 Specimens....36
Figure 5.17 Close-up of Corner of ASTM D1101 Specimens....36
Figure 6.1 Combined Bending and Tension Reaction Fram....37
Figure 6.2 Idealization and Geometry of Combined Bending-Tension Test....38

LIST OF FIGURES (con't)

Figure 6.3 Alignment Fixture 40
Figure 6.4 Bending-Tension Test Rig 41
Figure 6.5 Specimen BT1 Load-Displacement 43
Figure 6.6 Specimen BT1 Transverse Load vs. Axial Tension 44
Figure 6.7 Specimen BT1 FRP Strains 45
Figure 6.8 Specimen BT2 Load-Displacement 45
Figure 6.9 Specimen BT2 Transverse Load vs. Axial Tension 46
Figure 6.10 Specimen BT2 FRP Strains 46
Figure 6.11 Yielded Connection 47
Figure 6.12 Specimen BT3 Load-Displacement 48
Figure 6.13 Specimen BT3 Transverse Load vs. Axial Tension 48
Figure 6.14 Specimen BT3 FRP Strains 49

1. Introduction

1.1 Background

Guardrails are designed to protect motorists from certain dangers along the roadside, and are a common sight along roads and highways. The steel W-beam is the most commonly used guardrail because it is inexpensive, its behavior is well understood, it is durable, and it is easily installed. However, wooden guardrails are considered a more aesthetically pleasing alternative to steel W-beam guardrails along scenic highways.

This study focuses on the development of a cost-effective, timber guardrail that utilizes low-grade New England hardwoods such as red maple and beech. In order to be accepted for highway applications, the rail must be capable of passing the NCHRP Test Level 3 (TL-3) crash test (NCHRP 1993), and be easily installed using a standard post spacing of 1.83-m. Developing a rail to meet these requirements required significant effort on several fronts, including analyzing the response of the rail under vehicular impact, designing the rail section, fabricating rail specimens, evaluating the durability of the guardrail, developing a rail-to-rail field splice connection, and experimentally evaluating the structural performance of the guardrail. The remainder of this Section provides an introduction to timber guardrail systems and overview of this report.

1.2 Guardrail Overview

The design of traditional guardrail systems is a challenging problem due to the many factors that must be considered. The types of hardware and soil properties are critical to the performance of the system. The use of timber guardrails further complicates design due to wood's inherent brittleness in tension and the difficulty of designing and constructing strong timber-to-timber tension connections. These tension connections are necessary to transfer the large tensile loads between rail sections that are produced by vehicular impact.

Despite these obstacles, there are several wooden guardrails used on highways today. These include the Ironwood guardrail, which consists of logs with embedded steel channels, and the Merritt Parkway guardrail (also known as the steel-backed timber rail), which consists of a solid sawn beam of southern pine with a steel backing plate. In both of these wooden rail systems, the steel is used to carry the tension developed in the rail under vehicular impact. However, drawbacks exist in both of these timber guardrails. For logs with embedded steel channels, the logs can add undesirable variability in the shape and size of the rail, which can cause a vehicle to deflect above or below the rail more easily. While the Merritt Parkway rail does not suffer from this drawback, the cost of its relatively large solid sawn timbers is quite high, and the availability of large clear sections of structural softwood is decreasing.

Finally, both of these rail systems are relatively expensive and heavy, requiring the use of a small crane for installation of typical 3.66m-long rail sections.

The proposed guardrail designed and tested in this study is a reinforced glued-laminated (glulam) rail section fabricated from readily available mixed hardwoods (primarily red maple) and reinforced with a fiber-reinforced polymer composite material (FRP), as shown in Figure 1.1. This proposed rail is significantly lighter than available alternatives, easily installed, and potentially very cost-competitive.

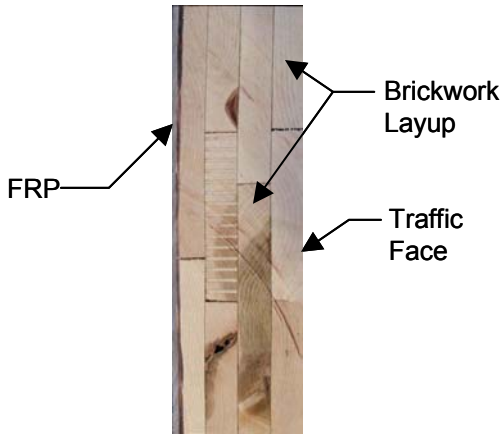

Figure 1.1 Glulam Guardrail Cross-Section

1.3 Report Organization

While FRP has been successfully used to reinforce glulam beams, the development of an FRP-reinforced timber guardrail posed unique challenges because of the use of hardwoods and the need for the rail to carry both flexure and tension. First, the structural response of the guardrail under vehicular impact had to be determined. The critical design parameters are the rail ductility and tensile capacity. The modeling of the guardrail to assess its structural response is covered in Section 2 of this report. Next, the rail cross-section had to be sized, and issues regarding fabrication and durability of the rail had to be addressed as discussed in Section 3. Section 4 details the bending tests conducted to access the flexural characteristics of the rail. Section 5 focuses on the design and testing of the bolted field splice connection that is critical for transferring the tension between adjacent sections of rail. Section 6 presents the development and results of the unique bending-tension tests that were designed to produce loads similar to those experienced by a guardrail under vehicular impact. Finally, Section 7 presents a summary of the work performed and the conclusions reached in this study.

2. Guardrail Modeling

2.1 Overview

The first objective of the analyses conducted in this study was to determine the maximum tensile – and to a lesser extent, flexural – loads that would be experienced by the FRP-reinforced glulam guardrail under a TL-3 crash test. The tensile forces are especially critical, since they must be transferred between 3.66m-long sections of rail via a field splice. The second objective of the modeling was to determine the effectiveness of the guardrail at containing and redirecting the impacting vehicle.

Since the 1960's a number of software programs have been developed in order to evaluate the behavior of guardrails systems as well as individual guardrail hardware items under vehicular impact. The current generation of guardrail models relies on explicit, nonlinear three-dimensional (3D) dynamic finite element software such as LS-DYNA3D (Patzner et al. 1998). Such 3D models are often used in the development of guardrail terminals, and use detailed 3D representations of the impact vehicle, the soil, the posts, and the rails. However, even with such complex models, it is very difficult to precisely model a reinforced glulam guardrail, since the 3D nonlinear stress-strain response of wood is not well understood. Further, it is extremely computationally costly to model the system using the appropriate material models in 3D finite element packages (Patzner et al. 1998), and the development of such models using available software would have required substantial time, expertise, and computer hardware that were not feasible given the scope of this project.

For these reasons, the response of the reinforced glulam guardrail design was evaluated using Barrier VII, a 2D dynamic finite element program originally developed at the University of California, Berkeley (Powell et al. 1973). Barrier VII has been widely used to evaluate guardrail systems (Taun et al. 1989; Rosson et al. 1997). Further, NCHRP Report 350 (1993) explicitly recommends its use for initial analyses, and notes that Barrier VII is useful for predicting the maximum loads on the components of a guardrail system.

Barrier VII is a relatively straightforward tool that incorporates flexural elements to model the guardrail, springs to model the posts, springs and dampers for modeling the soil, and is ideal for easily representing the geometry of the system. Barrier VII models the interaction of the vehicle, barrier, posts, soil, tires, and the vehicle sliding along the rail. The vehicle is treated as a mass body with springs that interact with the barriers. The system is modeled as a dynamic, inelastic, geometrically nonlinear, large deformation, two-dimensional structural analysis problem. Barrier VII also assumes elastic-plastic flexural response of the rail section with a final failure point, which is reasonably representative of the behavior of FRP-reinforced glulams with large amounts of reinforcement. Barrier VII is best used for situations when roll and pitch of the vehicle are negligible, which is assumed to be the case for the model used to validate the reinforced glulam guardrail.

2.2 Guardrail Performance Limits

It is important to understand how a guardrail system functions in order to understand its performance. During an impact, energy passes from the vehicle into the rail, from the rail through the blockouts, into the post, and into the soil. A single post cannot transfer all of the energy of the system into the soil, and the guardrail must remain intact, acting as a tension ribbon to mobilize a large number of posts; hence, the importance of the field splice connection between rail sections.

There are several different failure modes that can occur under vehicular impacts. Guardrails are designed specifically to pass the NCHRP 350 Test Level 3 crash test, and are not designed to withstand rarely occurring high-speed perpendicular impacts. The primary purpose of a guardrail is to redirect errant vehicles back onto the road without causing significant injuries to the occupants of the vehicle. Thus, if the vehicle ruptures the system, the guardrail has failed. If the guardrail system is too stiff, the vehicle may decelerate too rapidly causing injury to the occupants. Conversely, if the rail is not stiff enough, a pocketing failure can occur, where the guardrail system deforms such that the vehicle is not allowed to return to traffic. A pocketing failure usually results in high decelerations causing occupant injury (Patzner 1998). The most dangerous failure method of a guardrail system is snagging. Snagging occurs when part of the vehicle – usually the bumper or wheel – impacts a post, which does not fail. By snagging a post, the vehicle can be caused to flip over the barrier. Even if the vehicle does not flip, there is a danger from large impulse forces on the occupants due to the post impact. Thus, posts are designed so that during a crash the loads in the posts approach their capacity in the area of the impact, and thus if the vehicle does impact the post directly, the post will snap with minimal additional force.

2.3 Guardrail System Model

The crash test that was modeled was the NCHRP Report 350 Test Level 3-11 (NCHRP, 1993). The 3-11 test uses a 2000P vehicle, which is a 2000 kg pickup truck, typically a ¾ ton model that is one of the top two models in sales for the model year. This test was chosen as a basis for the worst-case scenario for all of the available Test Level 3 (TL-3) tests, and is intended to test the structural integrity of the rail section. The vehicle was assumed to strike the barrier at a speed of 100 km/hr and an angle of 25^{o}.

A 47.5m-long section of guardrail system was modeled as shown in Figure 2.1, which is greater than the minimum length of 30m specified for a TL-3 crash test. The minimum recommended length of guardrail that should be modeled is 45.7m (Calcote and Kimball 1978). W6X15 steel posts 1.8m-long and spaced 1.8m on center were assumed in the analysis. The terminal post at one end of the system was anchored, and the other end post was free to displace in the soil. An average value of 440 kN/m was used for the soil spring stiffness (Calcote, 1978). All of the Barrier VII models used a damping multiplier for rigid body rotation of 1.4. This damping factor was found to increase the stability of the model. The vehicle was assumed to impact the rail near the center, 22.86m from the end, half way between the two central posts. The reinforced glulam rail sections were modeled as 3.505m beams connected to the post, with 76mm-long by 13mm-thick steel plates connecting the rail sections to the post and adjacent rail sections at either end of the beams. This steel plate models the field splice connection detailed in Section 5 of this report. The moment capacity and bending rigidity of this steel plate is significantly smaller than

the reinforced rail sections, and therefore the plates effectively act as a yielding hinge in the system. This reflects the actual behavior of the splice connection.

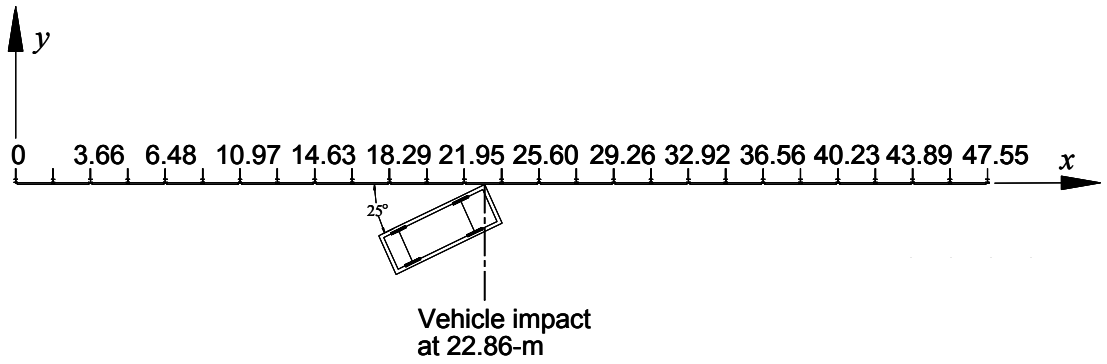

Figure 2.1 Guardrail System Layout (all dimensions in meters)

A transformed section analysis was used to determine the initial stiffness and the capacity of the guardrail cross-section. The properties used in the transformed section analyses were those published in the Wood Handbook (Forest Products Lab 1999) for red maple at 12% moisture content: an elastic modulus of 11.3 GPa, and a modulus of rupture of 92 MPa. The modulus of rupture is the maximum tensile stress in the wood at a bending failure (Forest Products Lab 1999). The FRP was treated as linearly elastic in both tension and compression. The modulus used for the FRP was the average tensile elastic modulus of 40 GPa for the Gordon Composites GC-67-UB unidirectional E-glass bar stock (Gordon Composites, Inc. 2001). The maple was assumed to have a linearly elastic stress-strain response in both tension and compression. While wood will yield under compression, no acceptable prediction of the yielding, experimental or empirical, was found to quantify the extent of yielding or yielding behavior of red maple. Therefore, for the initial stiffness and capacity analysis, the effect of compressive yielding of the glulam was neglected, and the yield moment for the rail section was taken as the moment that caused the first tension failure in the wood. All of the rail elements are assumed to have an elastic-plastic response by Barrier VII, which is reasonable for FRP-reinforced glulam with a large amount of reinforcing (Dagher and Lindyberg 2003).

2.4 Element Length Convergence Study

In order to determine the appropriate size of the reinforced glulam beam elements used to model the system, a convergence study was performed with several different element lengths. The convergence study was performed assuming a 114-mm deep cross-section with 3% FRP reinforcement, which was computed to have a yield moment of 73 kN-m and moment of inertia of 41.2×10^6 mm^4. While this is not the rail section ultimately selected and tested, it is sufficient for the purposes of the convergence study.

Guardrail element lengths of 914mm, 457mm, 228.5mm, and 152mm were considered. We note that when element lengths less than 152mm were used, the model became numerically unstable. In all models, a 76mm transition element was used at each end of the rail section to incorporate the splice connection. In order to incorporate smaller elements into the system without greatly increasing the number of elements and the run time of the program, an additional trial was run using 152mm elements from *x* coordinates of 18.288m to 32.918m and 457mm elements for the remainder of the system.

To approximate the worst case-loading scenario on the rail section, the vehicle impacted midway between posts at 22.86m from the beginning of the guardrail system and at an angle of 25°. The time step was held constant at 0.0001 s. The *x* direction displacements for the rail at 23.774m, which corresponds to the first post connection after the impact point, as well as the impact duration are compared to demonstrate model convergence. The effect of the difference in element length is cumulative, and is therefore more apparent toward the end of the simulation. Duration of the impact varies with element length, and therefore the results are only compared between the beginning of the simulation and 0.3 seconds after impact. The results of the element length convergence study for the *x* displacement at 23.774m are shown in Figure 2.2.

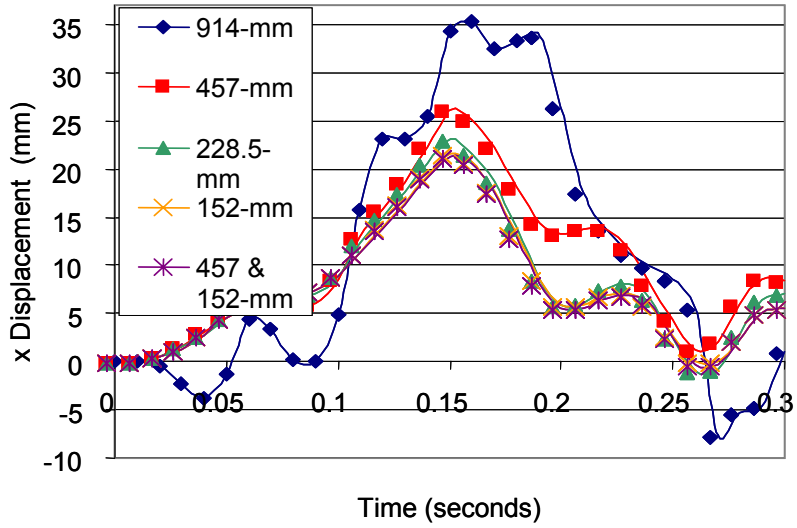

Figure 2.2: Displacement Convergence with Decreasing Element Size

Figure 2.2 shows that the model is clearly converging with decreasing element size. There is very little difference between the models with an element length of 152mm for the entire system and the model with 152-mm elements only in the area of impact, and the model with 228mm elements across the entire length varied only slightly from the model using the 152mm elements. Figure 2.3 shows the relation between guardrail element length and duration of the impact, and shows that the duration of impact clearly converges to a time of 0.31 seconds with element lengths of 152mm and 228mm. Further, the

model with 152mm elements near the impact region and 457mm elements elsewhere also has an impact duration of 0.31 seconds. Based on these convergence studies, the element size used in all further analyses of the system was the split system with the 152mm elements from *x* coordinates of 18.288m to 32.918m and 457mm elements elsewhere.

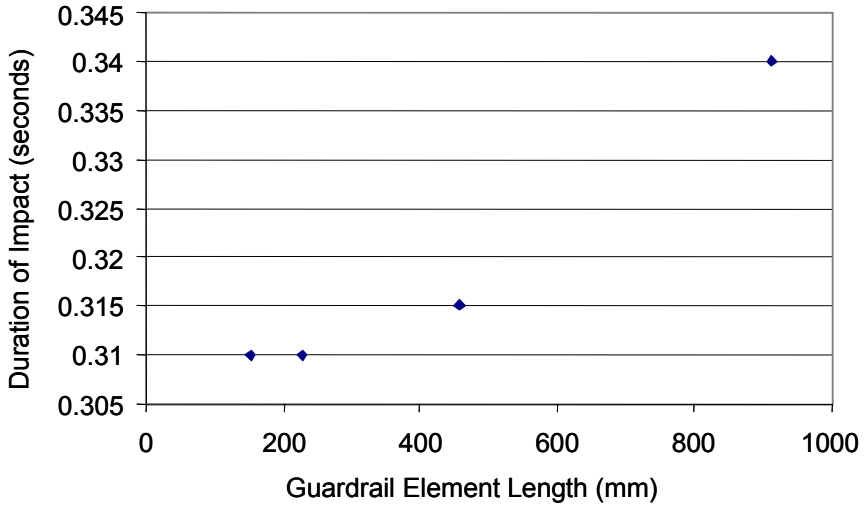

Figure 2.3: Convergence of Impact Duration with Decreasing Element Size

2.5 Time Step Convergence Study

In addition to the size of the elements used to model the system, a convergence study was performed to determine the most appropriate time step. The recommended time step for Barrier VII is usually between 0.01 and 0.005 seconds (Powell, 1973). However, smaller time steps may be necessary when the stiffness of the system and speed of the vehicle are increased. The stiffness of the reinforced glulam guardrail is higher than that of the standard W-beam and further, the TL-3 crash test speed of 100-km/hr is relatively high. Therefore, smaller time steps were investigated. Additionally, at time steps greater than 0.001 seconds the system became unstable and the vehicle loses contact with the barrier suddenly. Therefore, five time steps were used in the convergence study: 0.00001, 0.00005, 0.0001, 0.0005, and 0.001 seconds. The convergence analyses showed that the duration of the impact did not vary for any of the time steps considered, and the time step does not affect the behavior of the Barrier VII model within the limits considered. However, the larger time steps show more noise than the smaller time steps. This is most apparent when looking at the axial force in the guardrail splice connection at the first splice after the impact point as shown in Figure 2.4.

Figure 2.4 shows that at time steps of greater than 0.0001 s the axial load spikes at 0.13 s and appears to over-estimate the force in the splice. However, there is very little change in the maximum

force predicted for the remaining time steps. Based on the time step convergence analyses, a time step of 0.0001 s was used in the analysis of the reinforced glulam guardrail system.

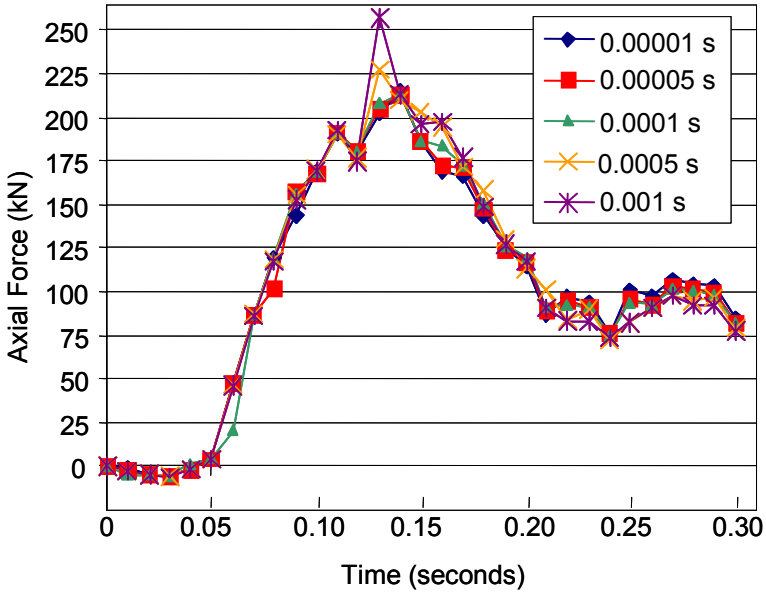

Figure 2.4: Convergence of Axial Force with Decreasing Time Step

2.6 Guardrail System Analysis Results

Detailed Barrier VII analyses were performed on three different reinforced glulam cross-sections to examine the effect of rail dimensions on performance and design forces. The original design was a 152-mm thick glulam with 3% reinforcement by volume. A lighter design consisting of a 114-mm thick glulam with 3% reinforcement by volume was also considered. The final glulam cross-section considered was a 76-mm thick glulam with a 3.5-mm thickness of reinforcement (4.7% by volume). Each of these cross-sections was analyzed with the transformed section method using the wood and FRP properties discussed previously to estimate the flexural stiffness and yield moments summarized in Table 2.1. In addition, a W-beam guardrail was also analyzed to provide baseline information on decelerations and lateral deformations in an acceptable, crash-tested rail system. The analyses indicate that the rails yield in bending at the impact point for all guardrail cross-sections, and a large axial force is induced in the rail as shown in Figure 2.5. Finally, Table 2.2 summarizes the results of the analyses, showing that the key response indicators of peak total deceleration and total lateral displacement of the rail are very comparable for the FRP-reinforced glulam rail and a traditional W-beam guardrail.

Table 2.1: Cross-Section Properties Used in Analyses

Cross-section	Bending Rigidity ($MN\text{-}m^2$)	Moment of Inertia ($10^6\ mm^4$)	Transformed Area (m^2)	Yield Moment (kN-m)	Weight (kg/m)
152mm	1.105	97.7	0.0428	130	20.8
114mm	0.467	41.3	0.0321	73	15.6
76mm	0.155	13.7	0.0225	40	10.4
W-beam	0.191	0.95	0.0013	8	10.3

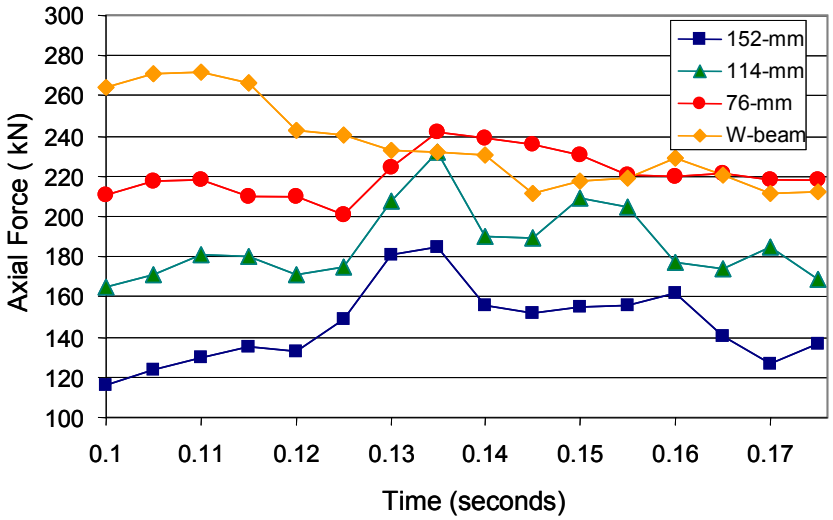

Figure 2.5: Maximum Axial Force in the Rail Splice Connection

Table 2.2: Summary of Barrier VII Analysis Results

Cross-section	Maximum Axial Force (kN)	Peak Long. Displ. (mm)	Peak Lateral Displ. (mm)	Peak Deceleration (g)
152mm	185	33.8	432	11.5
114mm	209	37.8	489	10.3
76mm	242	50.3	572	11.1
W-beam	271	93.5	627	11.2

2.7 Conclusions

Using the Barrier VII modeling tool, analyses were performed on several reinforced guardrail sections. These analyses predicted that the rail sections will reach the flexural capacity at the area of impact and that large tensile loads will be induced in the rail section due to impact. The vehicle decelerations and lateral displacements that occur during the vehicular impact are comparable to those for

the same rail system using a standard W-beam guardrail, which is indicative of good performance. The 76-mm thick reinforced hardwood glulam guardrail cross-section behaves most similarly to the standard steel W-beam, and therefore should be capable of passing the NCHRP 350 Test Level 3 crash test if it can be shown to have sufficient structural capacity. However, the 76mm thick guardrail section and splice connection must be capable of carrying a tensile force of approximately 240 kN. This large tensile force is the major design consideration in the development of the reinforced hardwood glulam guardrail, and requires the development of a specialized splice connection to transfer the force between adjacent rail sections as discussed in Section 4.

3. Guardrail Section Design, Fabrication and Durability Testing

The models detailed in Section 2 show that during vehicular impact, a guardrail experiences simultaneous bending and tension loads. This Section presents the design of a reinforced rail section to carry both bending and tension loads, focusing on the development of the guardrail cross-section. Also included are details of the durability testing and a cost estimate of the as-designed rail.

3.1 Reinforced Cross-Section Design

3.1.1 Sizing of Guardrail

The guardrail must be capable of catching all types of vehicles with bumpers of varying heights. The Ironwood rail discussed in Section 1 uses a 200mm diameter round timber to catch the vehicles, and the Merritt Parkway Guardrail (MPG) rail and the standard steel W-beam both use a rail depth of 305mm to catch vehicles. The reinforced hardwood guardrail developed here uses a glulam of depth 254mm, which is intermediate between that of the Merritt Parkway Guardrail and the Ironwood rail systems. This value was deemed sufficient to account for a variance in mounting height and to minimize the size, cost, and weight of the glulam section.

3.1.2 Material Selection

The species of wood to be used for the glulam was limited to the native New England species of eastern hemlock, red pine, red maple, and spruce-pine-fir. The species selected were red maple and mixed hardwoods. This selection was made based on ongoing research conducted at the University of Maine by Engineered Materials of Maine, which produces structural hardwood glulam beams using mixed hardwoods with a phenol-resorcinol-formaldehyde (PRF) resin system. A brickwork lay-up was chosen for the guardrail because it allows the use of multiple narrower pieces of wood to develop the full rail height of 254mm. The narrower lamination widths minimize the cost of the material needed to manufacture the guardrail sections. The use of a brickwork glulam also allows for the selective stacking

of laminates, with a low quality core and higher quality face laminations. Further, the red maple is an under-utilized species, and the wood that is used is low-grade material ripped from random width and length material that is essentially a waste product from hardwood mills.

It was also necessary to select the FRP used to reinforce the glulam. There are many different types of FRP that have been evaluated for bonding to wood, which can be divided into two main categories: wet layup and prefabricated. The wet layup method of FRP application involves applying a fabric of fibers across the surface that is being reinforced, and then infusing the fabric with resin. The two main methods of applying resin are hand layup and vacuum assisted resin transfer. Both of these methods result in a good FRP-wood bond but require an additional fabrication cost to attach the FRP. Also, achieving good quality control on FRP fabricated with wet layup methods can be troublesome due to the inherent difficulty of pulling a vacuum on the part being fabricated as well as maintaining fiber orientation during both hand layup and vacuum impregnation.

The second option is to use prefabricated FRP sheets. While the quality control for prefabricated sheets of FRP is very high, one drawback to the use of prefabricated sheets is the additional steps required to attach the FRP to the wood. Based on other work performed at the University of Maine (Lopez-Anido et al, 2001), it has been shown that it is possible to bond the FRP to softwoods using a Hydroxymethylated Resorcinol (HMR) primer and FPL-1 epoxy. Although the HMR and FPL-1 reinforcement system had not previously been used with hardwood glulams, the prefabricated FRP attached with the FPL-1 epoxy was chosen to reinforce the glulam guardrail based on its economy, ease of use and prior success with softwood reinforcement. A unidirectional E-glass epoxy Gordon Composites laminate was selected as the reinforcing material based on prior successful research performed at the AEWC Center. Based on the required dimensions of the FRP, the chosen laminate was the Gordon Composites GC-67-UB Unidirectional Fiberglass Bar Stock (Gordon Composites, Inc. 2001).

3.1.3 Lamination Scheme

A guardrail requires a balance of strength and stiffness. The guardrail must not rupture under an impact, must not form a pocket that can trap the vehicle, but must also be flexible enough to protect the occupants of the vehicle. If a guardrail is too stiff, it will not deflect sufficiently and will cause rapid decelerations of the vehicle occupants. Based on the relatively small lateral displacement and reasonable vehicular accelerations predicted by the Barrier VII analyses discussed in Section 2, a cross-section 152mm thick by 254mm deep with 3% reinforcement by volume on the non-traffic face was initially selected for the rail section. This thickness of 152mm was the same as that of the Merritt Parkway guardrail, which has been successfully crash-tested. However, this 152mm thick rail would be quite heavy (20.8 kg/m), since maple is denser than the southern pine or Douglas fir used in the Merritt Parkway

Guardrail. In order to reduce weight and further optimize material usage, a 76mm-thick cross-section was ultimately selected for testing. The 76mm deep cross-section has a mass of 10.3 kg/m, which is comparable with the weight of the W-beam rail. Additionally, the analysis results presented in Table 2.2 show that the lateral displacement and peak accelerations expected when using the 76mm thick rail are similar to those for the W-beam rail, which is known to perform. The reinforcement used on the 76mm deep cross-section was 3.5mm thick, giving 4.7% by volume of the 76-mm cross-section. While a smaller volume of reinforcement might give acceptable performance, 4.7% reinforcing was chosen to ensure ductile flexural response.

3.1.4 Brickwork Lamination Design

The glulam portion of the rail system consisted of four 19mm thick laminations. The laminations were used as either face or core laminations based on quality. Laminations with edge knots less than 1/3 the width of the cross-section and with a slope of the grain of less than 12.5% were classified as face laminations; any board which did not meet these criteria was used as core material. Placing the highest quality laminations on the faces of the glulam ensures that the highest quality laminations are in the area of maximum tensile stress and will also improve the wood-FRP bond. The brickwork lay-up was achieved by using combinations of two and three boards in random sequence as shown in Figure 3.1. No coincident seams were allowed between adjacent layers. The glulams were fabricated to 260mm wide and saw cut to give the 254mm dimension.

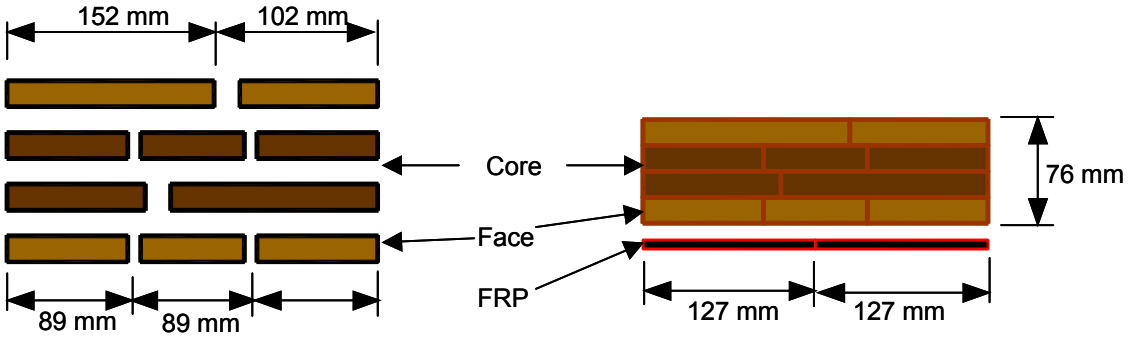

Figure 3.1: Glulam Brickwork Layup

3.2 Reinforced Glulam Fabrication

3.2.1 Glulam Layup

The guardrail sections were fabricated in 3.66m lengths. The wood for the glulams was purchased in random widths and lengths seconds from O & R Lumbra, Inc. in Milo, Maine. The first step in the fabrication process was to plane the wood surface and saw the wood to width. The wood was then graded and sorted. Next, finger joints were cut to allow multiple pieces of wood to be joined end-wise, producing

3.66m long boards. Finger jointing at the AEWC Center proved to be difficult due to quality and size issues with the finger jointer. Ultimately, boards wider than 120mm were finger jointed by Unadilla Laminated Products in Unadilla, New York, and the narrower boards were finger-jointed at the AEWC Center. The finger joints were glued using Ashland ISOSET UX-100 adhesive in the finger joint press at the AEWC Center.

Once the boards were finger jointed the next step in the fabrication process was to laminate the boards together. The boards were laminated in the cold clamps in the AEWC center. Due to the inconsistency in the thickness of the planed boards, the boards required additional compression to eliminate the slight gaps. The clamping pressure used was approximately 2,760 kPa, which is significantly higher than the pressure required when laminating softwood glulam beams. The resin was applied using a resin applicator in a constant coating of 0.341 kg/m^2. The laminations were then manually stacked. Figure 3.2 shows boards being fed through the resin applicator.

Figure 3.2: Resin Application and Lamination Stacking

The 3.66m long rail sections were fabricated in pairs. Once the boards of the glulam were coated with resin and stacked, they were flipped on edge so that the force was applied perpendicular to the bond line. A strip of plastic was placed between the two 3.66m long glulam rail sections and on the outside of the cold clamps. Two 51x157mm box steel sections and two 19mm by 157mm steel bars were stacked on both sides of the beam to distribute force across the outside of the beams. Once the beams were in place, they were clamped in the cold clamps with 36 –25.4mm diameter rods that were connected through the 51x51mm tubing with long 51mm nuts torqued to 332 N-m. Lateral bracing was also placed at the third

points to compress the rails, minimizing gaps between board edges and ensuring alignment of the boards. The specimens were cured under room temperature conditions for a minimum of eight hours.

3.2.2 Bonding FRP to the Glulam Rail

In order to bond the FRP to the glulam it was necessary to treat the surface of the glulam with the HMR coupling agent to allow the FPL-1 to bond to the wood. Once the glulams were fabricated, they were trimmed to size, and the bonding surface planed to provide a fresh surface and remove excess resin. The HMR was mixed and applied with a spread rate of 147 g/m^2 in accordance with the AEWC Center work instruction WI-01-05. The HMR was applied and allowed to cure for 16-21 hours before the application of FPL-1.

FPL-1 epoxy formulated in accordance with AEWC Center work instruction WI-01-05 was used to bond the FRP to the primed wood. The spread rate was 538 g/m^2, and the FPL-1 epoxy was applied by hand in an even coat across the treated surface of the beams. The FRP strips were wiped down with acetone to remove contaminates, then the FRP strips were placed on top of the FPL-1 coated surface. The glulams were then flipped and clamped with the FRP faces together and a strip of plastic between the FRP strips to prevent FRP strips from bonding together. Approximately 345 kPa of clamping pressure was applied to the bond surface using the cold clamps with 14-25.4mm rods torqued to 136 N-m. The glulams were then allowed to cure for a minimum of eight hours before unclamping.

Five 3.66m long specimens were fabricated using this process, and these specimens were then cut to length for the tests described in Sections 4-6 of this report. Since the FRP very rapidly dulls saw blades, the specimens were cut in a two-stage process. First, the FRP and approximately 4mm of the wood was cut with a diamond abrasive blade, and then the remaining wood was cut with a wood blade and trimmed to be even with the FRP.

3.3 Durability Testing

Before further testing could be performed, the durability of the reinforced glulam guardrail section needed to be qualified. Therefore, a set of durability and delamination tests was performed. These tests are important to qualify the behavior of the FRP-glulam bond in the exterior environmental conditions experienced by a guardrail. The test used to qualify the durability of the bonding of the wood to the FRP was the ASTM D1101 delamination test (ASTM 2002a). ASTM D1101 was also used to qualify the durability of the splice connection as discussed in Section 5.

Unlike the ASTM 2559 delamination test (ASTM 2002b), which is intended to qualify adhesive performance, ASTM D1101 is a quality control test to determine the integrity of a wood-to-wood bond. ASTM D1101 was selected over ASTM 2559 for two reasons. First, the ASTM 2559 test calls for the

fabrication of specialized specimens on which to perform the test, which would require additional time and expense. In contrast, the ASTM D1101 test is performed on a section of production run material, as a quality control test. The use of the actual cross-section was beneficial because of the large width of the cross-section and the reduction in time and materials associated with fabricating specialized specimens. Second, the FPL-1 epoxy has a glass transition temperature less than the temperatures at which steam is applied in the ASTM 2559 test; thus the effect of the ASTM 2559 test on the FPL-1 epoxy bond is unclear.

The ASTM D1101 Test Method A test consists of a wetting cycle and a drying cycle. The wetting cycle supersaturates the wooden portion of the specimens by submerging the specimens in water, pulling a vacuum for five minutes to remove the air from the wood, and then pressurizing the specimen to 552 KPa, forcing water into the wood structure. After the vacuum and pressure cycle, the specimens are dried in an oven at 60 ^{o}C for 24 hours. This wet-dry cycle is repeated three times to conclude the test. Between each wetting and drying cycle, the specimens are observed to denote any bond delamination.

Durability testing of the rail cross-section was performed on 76mm long rail sections. Ten tests were run on specimens cut from the same billets as the tension test specimens (see Section 5 for details). These tests showed minimal quantifiable delamination, less than 2.5mm in width. In all specimens the two separate sheets of FRP separated, and the individual sheets of FRP cracked at the gaps between pieces of wood due to stress concentrations. The areas of debonding were localized to these cracked areas. Since ASTM D1101 disregards delamination in the areas of damaged wood and checking, these small regions of debonding were considered insignificant.

3.4 Cost Analysis

In order to estimate the cost of the reinforced hardwood glulam guardrail, the fabrication and installation process was analyzed in detail.

The raw materials consist of the components used to manufacture the guardrail: hardwood glulam, reinforcement, FPL-1 epoxy, splice plates, and SIA E2119 epoxy. This estimate is based on the cost of a hardwood glulam commercially available at the time this study was conducted. While no 254mm by 76mm commercially available maple glulams were found on the market, Engineered Materials of Maine in Bangor, Maine produced a 241mm by 89mm glulam for $14.50 per meter. The volume cost of this glulam was applied to the 254mm by 76mm guardrail section giving a cost of $13.00 per meter. The cost of preservative treatment for structural lumber was estimated at 20% of the raw glulam cost, giving a price for the treated glulam of $15.65 per meter.

FRP reinforcement consists of two 127mm by 3.5mm bars produced by Gordon Composites, which costs approximately $37.20 per meter of length. In order to fabricate the splice connection for each

3.66m long rail section, two 254mm by 152mm by 13mm thick bonded steel splice plates, one 76mm by 76mm by 13mm thick steel plate to attach the rail to the intermediate post, and one 305mm by 254mm by 13mm thick plate are required. These plates will also need to be predrilled. Therefore, the raw material price of the steel was set to $2.20/kg to account for machining of the plates. The total weight of steel required for each 3.66m rail section is approximately 16.4 kg.

The cost of SIA E2119 epoxy is $20.20 per liter (L) when purchased in 18.9L pails. The cost for SIA adhesives epoxy was calculated for the same quantities detailed in Section 5, and assuming the same spread rate for all pieces steel bonded to the FRP-reinforced guardrail. The cost of the FPL-1 epoxy was estimated at $33.00 per kg from prior purchases made by the University of Maine AEWC Center.

The cost associated with the fabrication of the beams arises from bonding the FRP to glulam, bonding the steel plates to the FRP, and drilling holes through the SIA adhesive and reinforced glulam. Labor costs for bonding the FRP to the glulams, bonding the steel plates to the FRP, and installing the guardrails were based on a rate $33.40/hr for a laborer (Ogershock, 2002). It was estimated that with a cold clamp setup similar to the ones used to fabricate the test specimens, five man hours would be required to reinforce twelve 3.66m glulams. For installation of the guardrails, it was assumed that a three-man crew could install three 3.66m long guardrail sections in one hour, or one man hour was required per 3.66-m section. An additional labor expense is the drilling of the holes in the reinforced glulam. It was assumed that using a CNC machine, all of the holes in the reinforced glulam could be drilled in a maximum of 30 minutes. The cost of the labor involved was estimated based on a millwright at $47.71/hr (Ogershock, 2002). Finally, handling and shipping was estimated at 15% of the total material and labor cost. The installed cost of the reinforced glulam guardrail excluding posts and blockouts is estimated to be $118/m (see Table 3.1).

Table 3.1: Guardrail Cost Estimate

Item	Quantity	Unit Cost	Item Cost (per m)
Treated Glulam	1 m	$15.65	$15.65
FRP	1 m	$37.20	$37.20
FPL-1 Epoxy	0.14 kg/m	$33.00/kg	$4.62
SIA Adhesive	0.42 L/m	$20.20/liter	$8.48
Steel PL	4.5 kg/m	$2.20/kg	$9.90
Subtotal Materials			$75.85
Bond FRP	0.12 hrs/m	$33.40/hr	$4.01
Bond Steel	0.20 hrs/m	$33.40/hr	$6.68
Drill Holes	0.14 hrs/m	$47.70/hr	$6.68
Installation	0.27 hrs/m	$33.40/hr	$9.02
Subtotal Labor			$26.39
Shipping	--	--	$15.34
Total Cost			**$118.00**

4. Flexural Testing

In order to evaluate the stiffness and flexural capacity of the reinforced hardwood glulam guardrail sections in bending, two three-point bending tests were performed on 1.83m long specimens. The specimens used for these tests were cut directly out of the reinforced glulams that were fabricated in 3.66m billets as described in Section 3.

4.1 Test Setup

The specimens rested on two vertical supports with the center of the support pivots spaced at 1.68m apart. One of the supports allowed two degrees of rotational freedom, and the other support allowed only one degree of rotational freedom. A 152mm long, 13mm thick rubber pad was sandwiched between the specimen and each support to evenly distribute the support reactions to the specimen.

The load was applied at the center of the span by a 500 kN hydraulic actuator mounted below the floor. The actuator was attached to a loading frame above the floor with a section of 36-mm diameter Dywidag bar, and a 100 kN load cell was mounted on the load frame. A radiused hardwood load head with a pivot was attached to the 100 kN load cell. A rubber pad was placed between the load head and the specimen to raise the load head above the specimen and ensure that the point of load application remained at mid-span even under large deflections of the specimen. The test setup is shown in Figure 4.1.

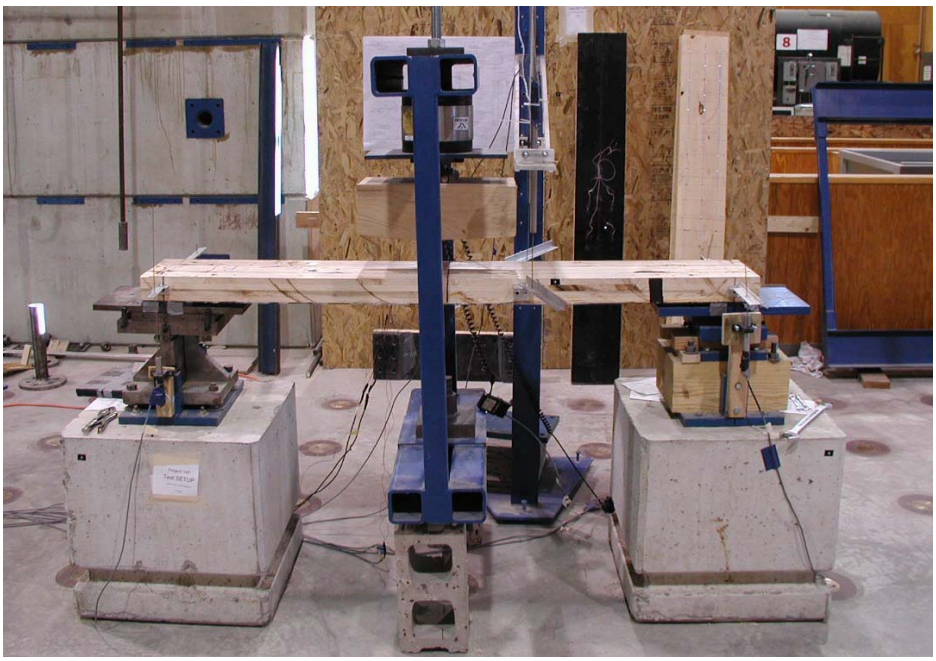

Figure 4.1: Flexural Test Setup

4.2 Instrumentation

Each specimen was instrumented with a 100 kN load cell to record load, a pair of LVDTs at the center of each support pivot to record vertical support displacement, and Measurements Group CEA-06-1250W-350 strain gauges to record the strain in the FRP (see Figure 4.2 for strain gage locations). The load and displacement of the actuator were output by the Instron controller as an analog output. This analog output was recorded in the data acquisition computer by a National Instruments PCI-6031E, 16 bit data acquisition card as a non-referenced single ended signal. The recorded actuator displacements included crushing of the rubber pads under the load head and on the supports. The effect of this crushing was removed from the data by quantifying the compressive response of the rubber pads.

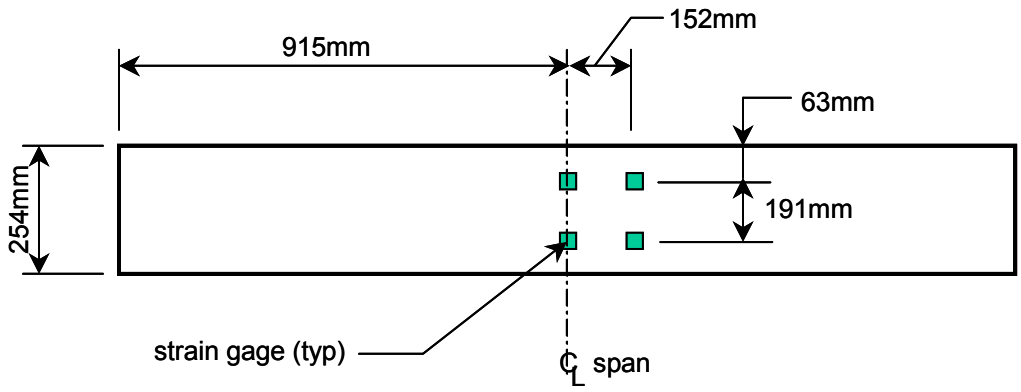

Figure 4.2: Strain Gage Locations

4.3 Test Results

The three point bending specimens are designated B1 and B2. The flexural tests were performed in displacement control at a rate of 13mm/min. The measured load-displacement response for B1 and B2 is shown in Figure 4.3.

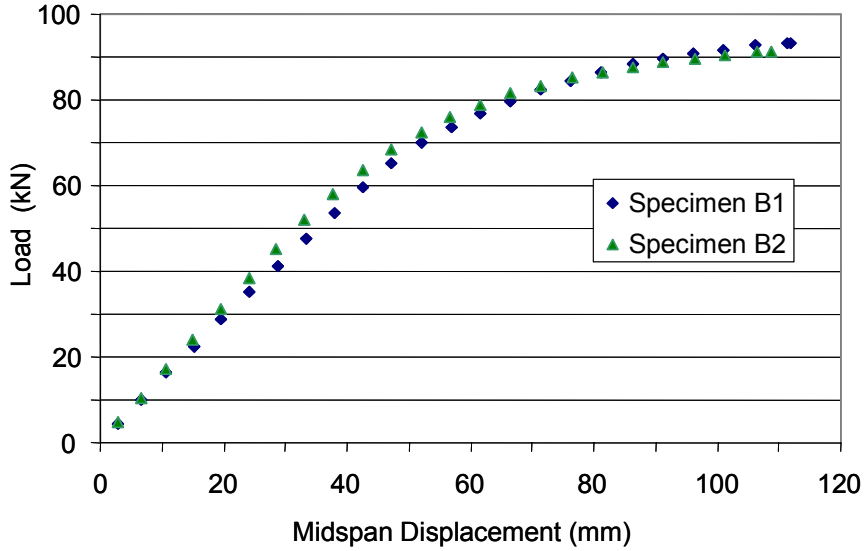

Figure 4.3: Flexural Load-Displacement Response

The displacements shown in Figure 4.3 are the load head displacements, corrected to account for the compression of the rubber pads placed under the actuator and at the supports. The effects of the 13mm thick pads on the supports were removed from the load head displacement by subtracting the average of the four LVDT readings at the pivots of the beam from the load head displacement. To account for the compression of the load head and rubber pad under the load head, a simple test was performed where the rubber pad on an incompressible base and compression was applied through the load head to determine the load-displacement relation. While this test does not exactly model what occurs during the flexural test because there is a high degree of curvature in the guardrail specimen in the area of the load head, it was felt to be a reasonable approach.

The compression load-displacement response obtained from the rubber pad and load head is shown in Figure 4.4. The maximum load applied to the load head and rubber pad equaled or exceeded the maximum load applied to the specimens discussed here and in Section 6. All of the reported displacement values in this Section and in Section 6 have been corrected to remove the effects of the load head and rubber pad.

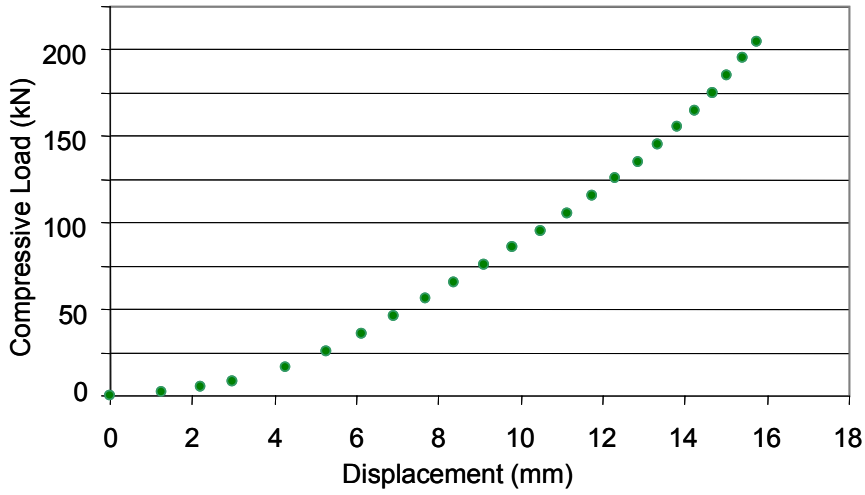

Figure 4.4: Compression Response of Load Head and Rubber Pad

The maximum load for specimen B1 was 93 kN at a displacement of 111mm. The maximum load carried by B2 was 91 kN at a displacement of 109mm. The failure loads and corresponding displacements for the two tests were within 3% of each other. The behavior of the load-displacement curve is nonlinear due to the high percentage of FRP reinforcing (4.7%), which caused significant flexural compressive yielding of the wood at the high loads. This yielding is also evident in the measured load-strain response shown in Figure 4.5. The specimens showed very similar load-strain behavior, and the measured strains did not approach the failure strain of the FRP (approximately 23,000 microstrains).

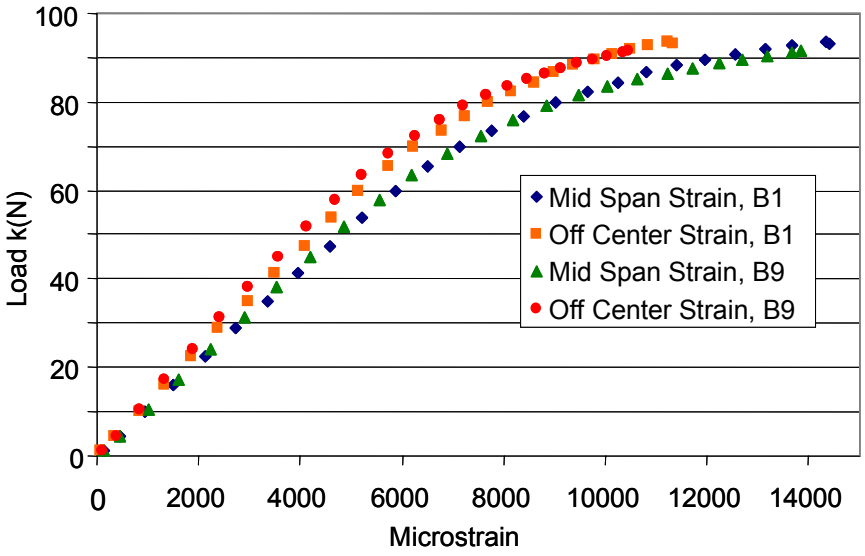

Figure 4.5: Load-Strain Response

In both specimens, the tensile laminations of the reinforced glulam failed, causing delamination of the FRP from the glulam. However, the delamination did not occur in the FPL-1 epoxy bondline, but was an inter-laminar shear failure in the FRP. The tensile lamination in specimen B1 failed at a finger joint approximately 75mm off center, while specimen B2 exhibited tensile failures over a larger portion of the glulam as shown in Figure 4.6(c).

(a) Failure of B1

(b) FRP Delamination in B2

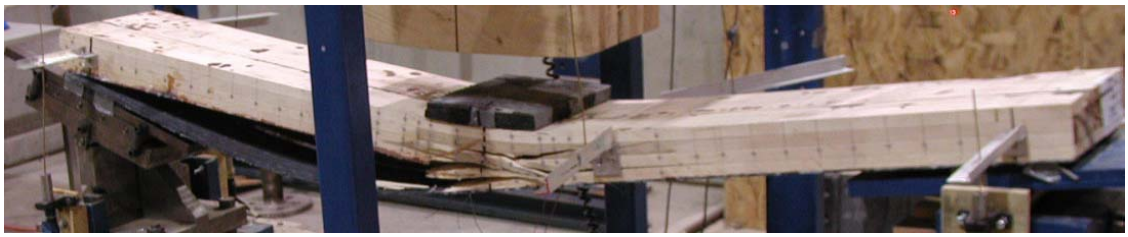

(c) Failure of B2

Figure 4.6: Flexural Failure Modes

4.4 Determination of the Elastic Modulus and Effective Section Properties

In order to have accurate input for the modulus of elsticity, area, and moment of inertia for further simulations, the the modulus of elasticity of the wood glulam was back-calculated from the three point bending test data. The effective moment of inertia was then found by the transformed section analysis method, once the modulus of the wood was known.

Using the load-displacement relation presented in Figure 4.3, the bending rigidity, *EI*, of the reinforced hardwood glulam guardrail section was calculated using the standard equation for the displacement at the center of a simply supported beam with a concentrated load applied at its center.

$$\delta_c = \frac{P \cdot L^3}{48 \cdot EI} \tag{4.1}$$

In Equation 4.1, δ_c is the mid-span deflection, P is the applied transverse load, L is the span length, E is the modulus of the wood, and I is the transformed section moment of inertia. Equation 4.1 can be re-arranged to give Equation 4.2.

$$EI = S \cdot \frac{L^3}{48} \tag{4.2}$$

In equation 4.2, S is the slope of the linear range of the experimental load-displacement curve, which was taken between 9 and 53 kN of applied transverse load. An average *EI* was determined for specimens B1 and B2 using Equation 4.2.

To determine the elastic modulus, *E*, an initial guess for *E* was assumed, and the corresponding *I* was computed using the transformed section method. A new *E* was then calculated by dividing the average experimental *EI* computed according to Equation 4.2 by the calculated value of *I.* This process of updating the estimate for *E* was repeated until it did not change significantly. Ultimately, *E* was found to be 10.3 GPa, the transformed area was found to be 0.023m^2, and the transformed moment of inertia was computed as 14x10^6 mm^4 (both expressed in terms of wood).

4.5 Summary

Both of the three point bending tests yielded similar results. The failure load of specimen B1 was 93 kN at a displacement of 111-mm. The failure load of specimen B2 was 91 kN at a displacement of 109-mm. Both tests displayed nonlinear load-displacement and load-FRP strain relations due to the compressive yielding of the wood at higher loads. The FRP-glulam bond proved effective at high loads, and in both tests layers of FRP remained bonded to the glulam after the flexural failure of the guardrail specimens. From the load-displacement results and a transformed section analysis, the modulus of the wood was found to be 10.3 GPa, which is 8% less than the published value for red maple of 11.3 GPa (Forest Products Lab 1999). One possible explanation for this discrepancy may be the gaps between

boards that were present in the brickwork glulam. The transformed area of the cross-section was found to be 0.023m^2 and the transformed moment of inertia of the guardrail section was found to be 14x$10^6$$mm^4$ (both expressed in terms of wood).

5. Development and Testing of Field Splice Connection

The analyses of Section 2 show that vehicular rail impacts induce not only large bending moments in the rail, but also tensile forces as large as 240 kN. These tensile forces must be transferred throughout the length of the rail system and distributed into the posts. In order to transfer the tension between the 3.66m-long reinforced glulam rail sections and allow for easy installation, a specialized splice connection was developed. Field serviceability requirements dictate that the splice connection between rails permit the easy replacement of individual rail sections. This section covers the development, fabrication, and testing of the splice connection.

5.1 Overview of Splice Connection

The easy replacement of damaged rail sections requires the use of field-bolted connections to transfer tension through the splice. The simulations of Section 2 indicate that the tensile force in the connection can reach 240 kN. Further, the FRP is expected to act as a continuous tension ribbon and carry the majority of the tensile load once the guardrail's flexural strength is exceeded. This requires that the splice connection effectively transfer the tension between adjacent pieces of FRP. Unfortunately, both the glulam and the unidirectional FRP used in the reinforced rail section have relatively low shear strength, which limits the load that can be transferred through a conventional bolted connection. This required the development of a unique connection.

We note the fiber orientations of the laminate could be varied to increase the shear capacity of the FRP reinforced glulam; however, this reduces the tensile strength and the stiffness of the rail, which is undesirable. It is also possible to add additional FRP between layers of wood or on the exterior of the laminate to increase the shear capacity as demonstrated by Soltis et al. (1998) and Chen (1998). This process essentially increases the shear strength of the laminated beam in the connection area, thus increasing the bolted connection capacity. However, this process is labor intensive, costly, and may not provide the needed increase in shear capacity. For these reasons it was necessary to explore an alternative method to transfer the tensile force between glulam rail sections.

The ideal connection would combine the easy installation of a bolted connection and distribute the tension into the rail via shear over a reasonable area of the rail section. Boone (2002) demonstrated that it is possible to transfer large tensile forces from metal to FRP through shear in a thick epoxy bond line. The chosen splice design combines this concept of a thick epoxy bond with the bolted connection by

epoxy-bonding a steel plate to the FRP, and relying on bolts to transfer shear between two pieces of steel. The steel-to-FRP bond is shop-fabricated, which allows the rail sections to be easily bolted into place in the field. Figure 5.1 shows the general configuration of the splice connection.

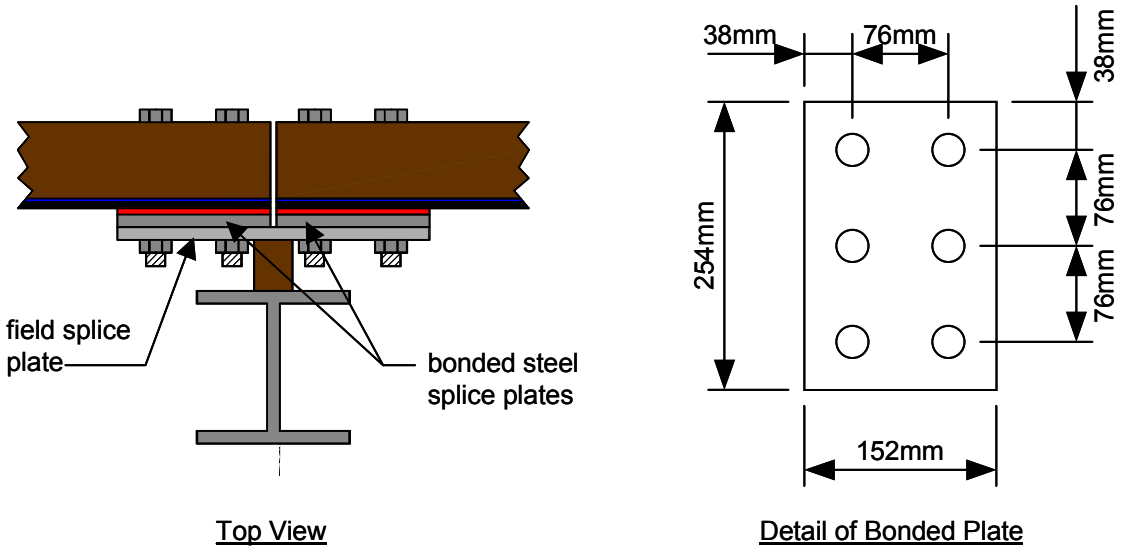

Figure 5.1: Splice Connection

There were four requirements for the epoxy adhesive. First, the adhesive must provide shear strength greater than 240 kN, the maximum predicted tensile load, with a reasonable bond area. Second, the adhesive must be able to withstand impact loading and exhibit a non-brittle failure mechanism. Third, the adhesive must not degrade under exterior exposure conditions. Finally, the adhesive must be economical. Based on the work of Boone (2002), Sovereign Specialty Chemicals, SIA Adhesives E2119 epoxy was selected for use in the splice connection. This adhesive is rated to withstand impact loadings, does not exhibit a brittle failure mode, provides a high shear strength at a reasonable bond line thickness, and its performance is not sensitive to small variations in bond line thickness. Sovereign Specialty Chemicals donated all of the E2119 epoxy used in this study.

Once the epoxy was selected, the appropriate bond length and bolt pattern needed to be determined. When determining the number and size of the bolts it was important to consider the ease of field installation of the guardrail as well as the capacity. The standard W-beam guardrail uses eight 13mm diameter A325 bolts to splice rail sections. Due to the thickness of the steel W-beam, the steel W-beam will locally yield before the bolts fails in shear. The reinforced glulam guardrail splice connection uses six 19mm diameter, A490 bolts to ensure that the steel-FRP epoxy bond would fail before the bolts. The combined ultimate design strength of the 19mm diameter A490 bolts in shear, assuming threads in the

slip plane, is about 530 kN (AISC 2002), which is in excess of the loads predicted. Additionally, the steel plate bonded to the FRP was 13mm thick to ensure that the steel plate would not fail before the bolts.

Due to uncertainty regarding response of the SIA E2119 adhesive under the eccentric shear load and the effect of the bolts on the bond capacity, the required bond area could not be accurately calculated. Geometric constraints were used to set the lower limit for the size of the plate. The minimum size of the steel plate that was bonded to the FRP was set at 152 X 254 X 13mm as shown in Figure 5.1. The 254mm dimension corresponds to the depth of the guardrail cross-section and the 152mm length allows the use of a 76mm bolt spacing and 38mm edge distance, which ensure easy constructability. Initial plans called for testing specimens with bond lengths longer than 152mm, but this proved to be unnecessary due to the excellent performance of the connection with a 152mm bond length as detailed later in this Section.

5.2 Fabrication of Splice Connection Specimens

The specimens tested in tension were 838mm-long reinforced glulams cut from the 3.66m billets. The first step in the fabrication of the splice connection test specimens was to mill the bolt pattern into the steel plates, leaving approximately 2-mm of steel left in the bottom of the hole with a 22-mm center cutting end mill. Next, a surface treatment was applied to the steel. The purpose of the surface treatment is to eliminate oxides from the bonding surface, as well as to add texture to increase mechanical interlocking of the epoxy and the steel. The same surface treatments developed by Boone (2002) for bonding FRP to aluminum were considered even though steel is less sensitive to oxidation than aluminum: hand sanding, grit blasting, and acid etching. While Boone (2002) showed that acid etching provides the highest quality bond, it is relatively expensive. Hand sanding was also ruled out since it requires a large amount of labor and it produces relatively low bond strength. Ultimately, grit blasting was used to prepare the surface of the splice connections for bonding, since it allows for a high strength bond with minimal additional labor and expense. One disadvantage of using grit blasting is that the surface has a limited life before it oxidizes. Boone (2002) found that the maximum surface life of aluminum was three hours. While steel oxidizes slower than aluminum, the same three-hour surface life was assumed to apply to the steel to ensure bond quality.

After grit blasting, the surface was wiped with acetone to remove dust and contaminates. It was also necessary to hand sand the FRP and wipe the surface with acetone. The same three hour surface life was assumed to apply to the FRP. Next, 162g of SIA E2119 epoxy was applied to each bonded steel splice plate, and the plates were pressed onto the FRP and left to cure for three days. Finally, the holes were milled through the remaining steel and the FRP using a 22mm center cut end mill. Holes were drilled through the wood with a 22mm spade bit.

5.3 Connection Testing Program

Six splice connection tension tests were run to determine the capacity of the connection. The primary variable in the test program was the torque load in the bolts. Bolt torque is important because yielding and failure of the steel-FRP epoxy bond under both shear and peeling stresses initiate the failure of the splice connection, and the bolts reduce the effect of peeling stresses by compressing the bond.

Unfortunately, bolt torque is difficult to predict in a bolted wood connection due to creep in the wood perpendicular to the grain, which can be significant. One similar application where creep perpendicular to the grain has been measured is in stress laminated bridge decks, where vertical deck laminations are transversely pre-stressed using threaded steel rods. For such decks, losses in tensile force as high as 80% are observed in the steel rods due to creep when the deck is stressed only once during construction. However, if the prestressing rods are re-stressed twice, once one week after construction and once 5-7 weeks after construction, the maximum prestress loss will be limited to 60% (Ritter 1992).

These relationships were assumed to give a reasonable approximation for typical creep losses in bolt load torque in the guardrail splice connection. The maximum bolt torque was fixed at 136 N-m, which was just enough to crushing of the glulam in the area of the bolts and washers during tightening of the bolt; two tests (specimens T1 and T2) were run with the bolts torqued to this value. Two tests (specimens T3 and T4) were conducted with a bolt torque of 54 N-m, which corresponds to a 60% loss of prestress. Finally, a worst-case scenario was also considered, with two tests performed assuming a loss of 80% of the initial bolt torque, giving a bolt torque of 27 N-m (specimens T5 and T6).

5.3.1 Tension Test Setup

The tests were performed on the 1780 kN Baldwin-Satec test frame in the Hybrid Structures Lab in the basement of Boardman Hall. An eccentric tension load was applied to each specimen to simulate the tension in an actual guardrail splice connection. The length of the test specimen was 838mm. The specimen was bolted to a 25mm-thick connection plate that was gripped by the Baldwin test frame. The connection plates were the same width as the test specimen (254mm), and had a bolt pattern matching that of the splice connection (see Figure 5.1). Figure 5.2(a) shows a specimen in the Baldwin test frame.

The tests were run in load control at a load rate of 22 kN/min until the load approached the anticipated failure load, and then the system was switched to displacement control. A load rate of approximately 22 kN/min was also maintained during the displacement control portion of the test. Due to safety concerns, as the load approaching the failure load of the bolts, the load limit was set to 500 kN, which was slightly less than the ultimate design shear strength of the six bolts. In order to limit the risk to personnel and equipment in the event of bolt shear failure, a safety frame was constructed around the specimen to deflect the bolts in the event that they sheared during the test.

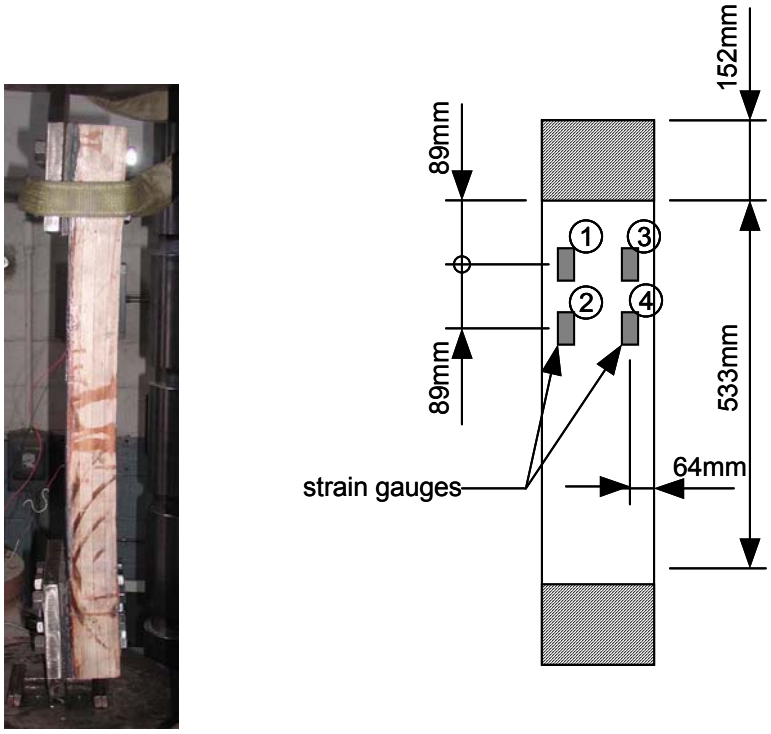

a: Specimen in the Test Frame b: Strain Gauge Locations

Figure 5.2: Typical Tension Specimen

5.3.2 Instrumentation

Load, crosshead position, and strain at four locations on the FRP were recorded during the tensile tests. The load and crosshead position were recorded directly from the Satec controller on the Baldwin test frame. Due to problems with the Satec's recording of data, load was manually recorded from the Satec controller screen display every 30 seconds. This load data was then correlated via time with displacement and strain data acquired by a separate data acquisition system.

Due to difficulties measuring strains in wood, the strains were only in the FRP with Measurements Group CEA-06-125UW-350 strain gages. These gages have a resistance of 350 ohms, which is necessary to prevent excess heat generation. For redundancy, four gages were bonded to each specimen at the locations shown in Figure 5.2(b).

5.4 Test Results

5.4.1 Results for 136 N-m of Initial Bolt Torque

The load rate used for specimen T1 was 22 kN/min until a load of 333 kN was reached, and then a displacement rate of 0.25 mm/min was used. The load rate resulting from the displacement rate of 0.25

mm/min was approximately 4 kN/min, which was significantly less than the target load rate of 22 kN/min. The displacement rate was increased for the later tests to more closely approximate the 22 kN/min target load rate. Three of the strain gauges were damaged during installation of the specimen, and one strain gauge 2 was functional during the test. Figure 5.3 shows the measured load vs. strain for specimen T1.

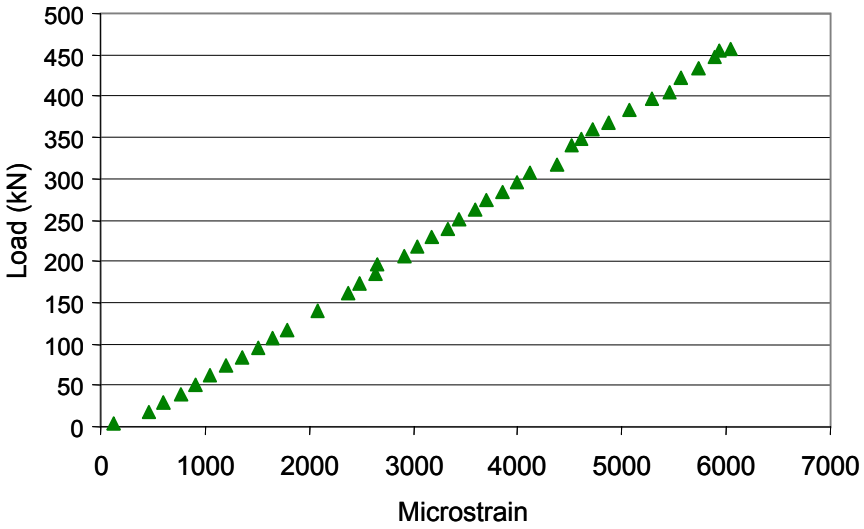

Figure 5.3 Load-Strain Relation for Specimen T1

As seen in Figure 5.3, the load-strain relation was essentially linear. The slope of the load-strain relation was computed between the loads of 45 kN and 333 kN to minimize the effect of connection slippage and signal noise. The slope was found to be 80 N/microstrain.

Figure 5.4 shows the load-deformation relation for specimen T1. The initial response up to a load of about 100 kN was nonlinear due to initial slip of the bolts and Baldwin clamps. The second region from approximately 100 kN to 200 kN exhibits linear load-deformation response. The remainder of the curve is nonlinear due to yielding of the steel-FRP epoxy bond. The peak load carried by specimen T1 was 462 kN. Near the peak load, localized failures of the wood-FRP epoxy bond caused uneven loading of the FRP. This in turn caused longitudinal shear failures and slip planes in the FRP.

This failure of the FRP in shear parallel to the fiber direction was unexpected. However, the failure of the bolted connection occurred as anticipated with a plug-type tear out in the reinforced glulam after yielding of the steel-FRP bond. Figure 5.10 shows the plug tear out failure of specimen T1 in the wood-FRP composite. It is important to note that despite the plug failure the connection remained intact and still carried a significant load.

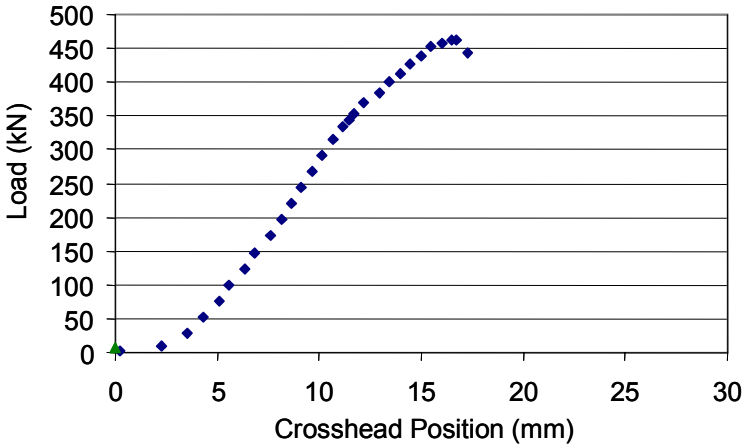

Figure 5.4 Load vs. Crosshead Position for Specimen T1

For specimen T2, a new system was used to protect the strain gauges while installing the specimen, and all four of the strain gauges remained functional for most of the test. In contrast to specimen T1, specimen T2 did not smoothly ramp up to a peak load and then fail. Instead, as the load approached 400 kN the connection slipped, losing some load, and then resumed gaining load. The slippages in the connection are clearly seen in Figures 5.6 and 5.7 as jumps in the load-strain, and load-position curves. There were several small slippages before the peak load was reached.

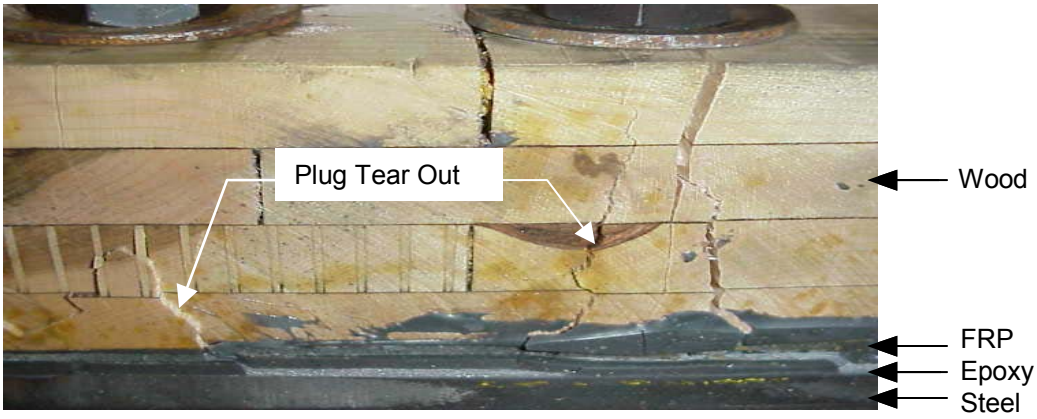

Figure 5.5 Bolt Plug Tear-Out for Specimen T1

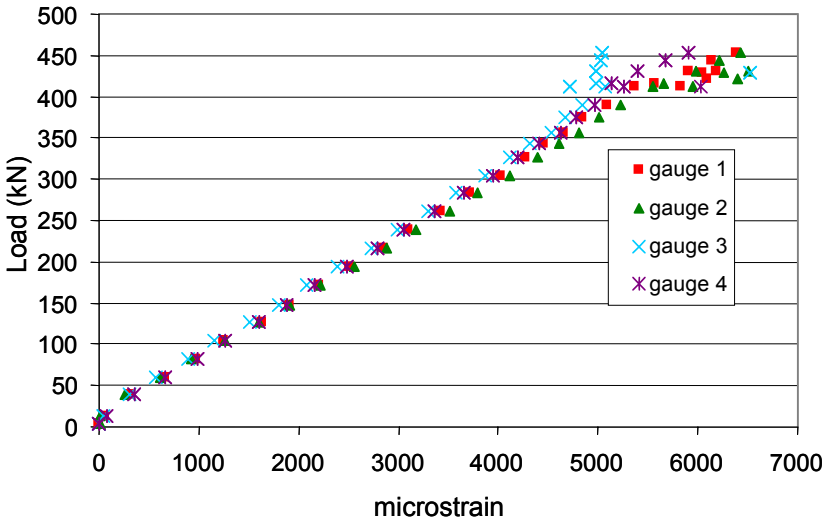

Figure 5.6 Load-Strain Relation for Specimen T2

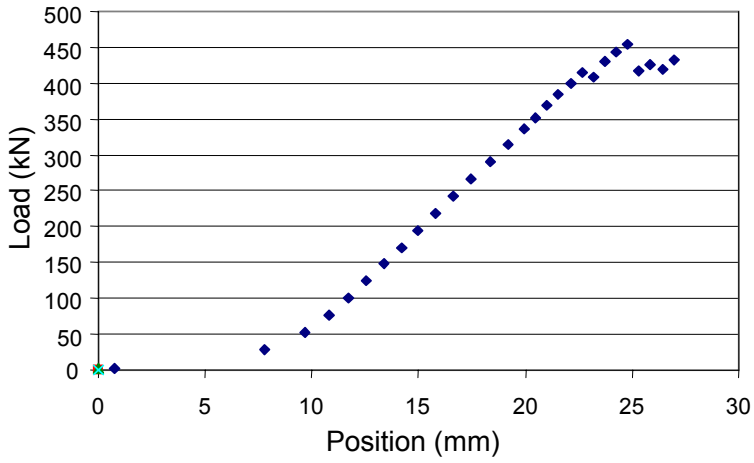

Figure 5.7 Load vs. Crosshead Position for Specimen T2

As seen in Figure 5.6, the load-strain relation is linear until the first connection slippage. After the first connection slippage the load-strain relation became noisy due to the repeated load values, damage to the gauges, and an uneven redistribution of load over the cross-section. The average slope of the load-strain relation between 45 kN and 333 kN for all four gauges is 72.5 N/microstrain. The maximum deviation from this average for any gauge is 4.5%.

It is important to note from Figure 5.6 that both strain gauges 3 and 4 encountered damage during the first slippages of the connection due to longitudinal shear cracks in the FRP in the area of the strain gauges similar to what was observed in specimen T1. The strain gauges on the opposite side, 1 and 2, remained intact throughout the test.

Despite the slippages in the connection and the loss of load, the connection remained intact and still maintained substantial tensile capacity. The final failure was a yielding of the steel-FRP bond, resulting in bond slippage and a shear plug-type of failure of the reinforced glulam similar to that observed for specimen T1. The ultimate load for specimen T2 was 463 kN.

The overall performance of the two tests performed at an initial bolt torque of 136 N-m was better than anticipated, with both specimens carrying approximately 1.9 times the 240 kN anticipated load on the connection.

5.4.2 Results for 54 N-m of Initial Bolt Torque

Specimens T3 and T4 were tested with an initial bolt torque of 54 N-m. Specimen T3 performed similarly to specimens T1 and T2, which were tested at 136 N-m of initial bolt torque. However, T3 exhibited a smaller region of nonlinear behavior before the ultimate failure of the connection than was observed for specimens T1 and T2. The load-strain relation is shown in Figure 5.8.

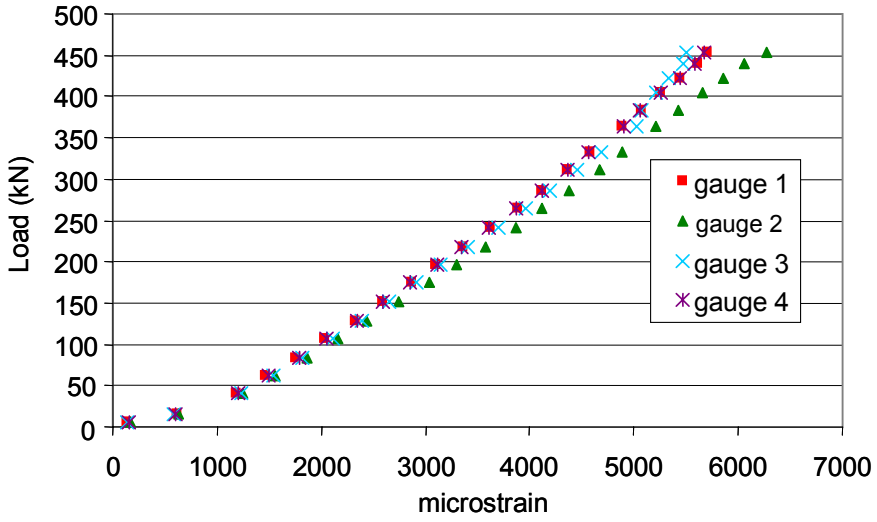

Figure 5.8 Load-Strain Relation for Specimen T3

The average slope of the load-strain curve between 45 kN and 333 kN was found to be 84.7 N/microstrain, and the largest variation from the mean slope was 5.4% for any one gauge. The abrupt failure of specimen 4 can be seen in the load-deformation relationship shown in Figure 5.9.

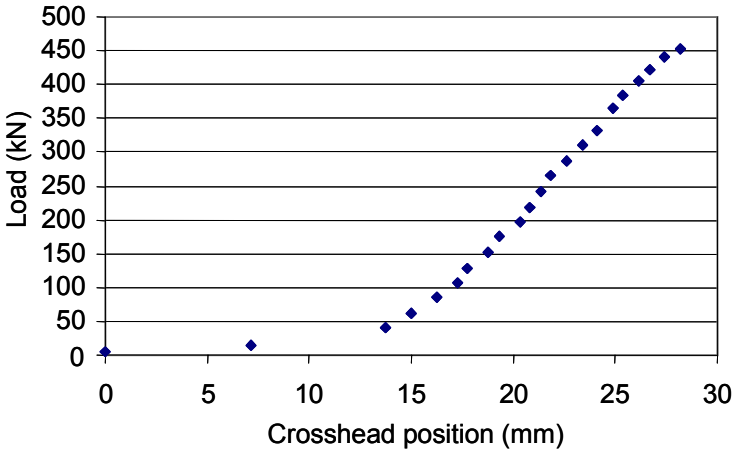

Figure 5.9 Load vs. Crosshead Position for Specimen T3

The maximum load for specimen T3 was 452 kN, which is only 2.2% less than the average capacity of the specimens tested at 136 N-m of initial bolt torque. There were no large slippages in the connection preceding the failure in specimen T3 as occurred in the previous tests at 136 N-m of initial bolt torque. The ultimate failures observed were similar to those of specimens T1 and T2, with the steel-FRP bond yielding accompanied by a shear plug failure in the reinforced glulam. There were also longitudinal shear cracks in the FRP caused by the redistribution of the load in the failure process.

The second specimen tested at an initial bolt torque of 54 N-m, specimen T4, had a lower steel-FRP bond quality than any of the other specimens tested. The bond was observed to be of poor quality before the test was performed. Despite the poor bond quality, the load-strain relation for the splice connection was still linear as shown in Figure 10.

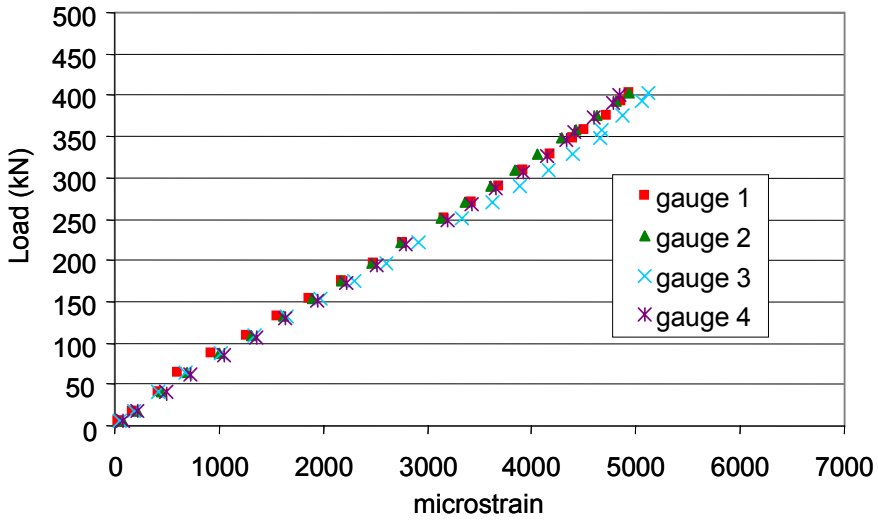

Figure 5.10 Load-Strain Relation for Specimen T4

The average slope of this load-strain relation between 45 kN and 333 kN for specimen T4 is 77.5 N/microstrain, slightly higher than the previous test performed at an initial bolt torque of 54 N-m. Figure 5.11 shows the load-deformation response for specimen T4.

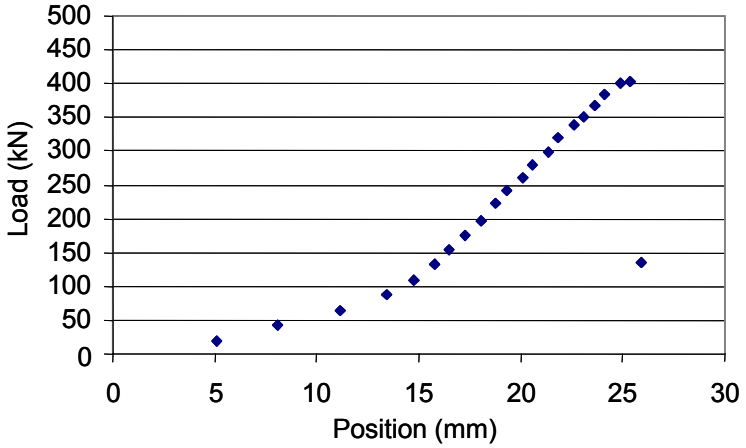

Figure 5.11 Load vs. Crosshead Position for Specimen T4

The shape of the load-strain curve is similar to that observed for specimen T3. Further, despite the low bond quality, the peak load carried by the connection was 403 kN, which is only 11% lower than that carried by specimen T3 and approximately 1.68 times the desired capacity of 240 kN. The ultimate failures observed were similar to those of the previously tested specimens, including slippage of the steel-FRP bond resulting in plug-type shear failure around the bolts.

The overall performance of the connections tested with an initial bolt torque of 54 N-m was quite good. The average capacity of the connection was decreased to 427 kN, only 7.5% less than that observed for the specimens tested at an initial bolt torque of 136 N-m, despite the poor bond quality of the second specimen.

5.4.3 Test Results for 27 N-m of Initial Bolt Torque

To determine the effect of extreme bolt torque loss on the tensile capacity of the splice connection, two tests were performed at an initial bolt torque of 27 N-m. This torque level represents almost total relaxation of the bolt load. The first of the specimens tested at an initial bolt torque of 27 N-m, specimen T5, achieved a peak load of 392 kN. This is a significant decrease from the specimens tested at a higher initial bolt torque. The relationship between load and FRP strain for specimen T5 is shown in Figure 5.12. The average slope of the load strain relation between 45 kN and 333 kN for specimen T5 was 83.3 N/microstrain.

Figure 5.13 shows the load-deformation response of T5, and indicates that the connection yields only slightly prior to failure. The failure was observed to have more slippage of the steel-FRP bond and the associated plug-type shear failure in the wood-FRP glulam than in the tests performed at higher levels of initial bolt torque.

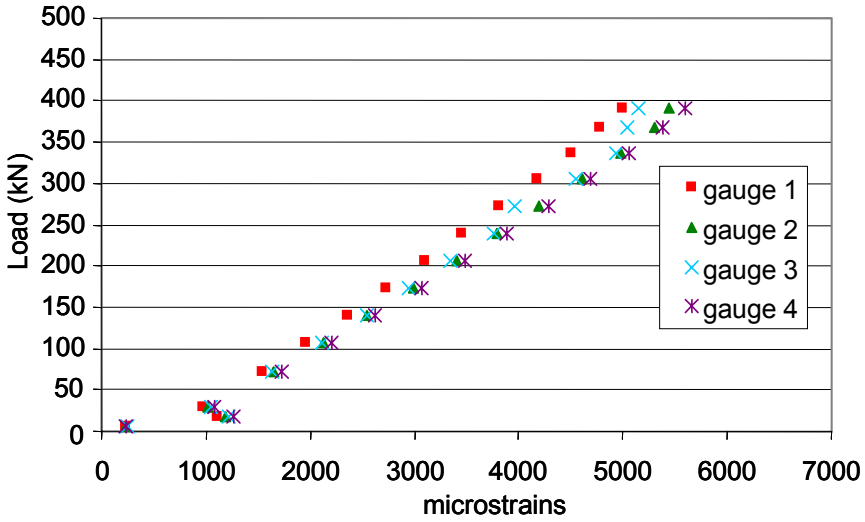

Figure 5.12 Load-Strain Relation for Specimen T5

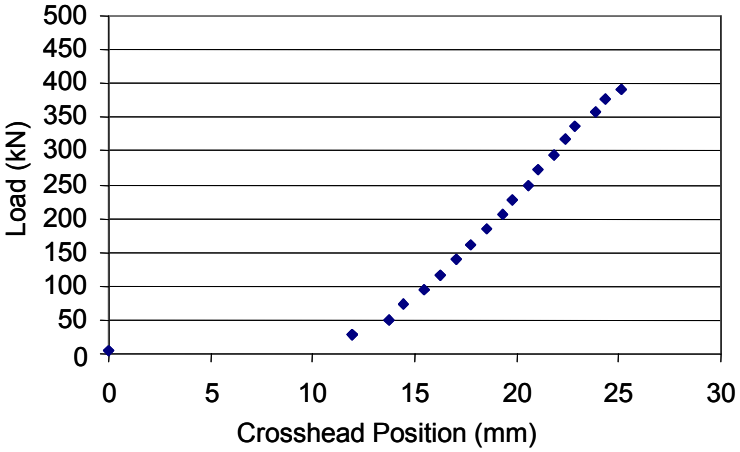

Figure 5.13 Load vs. Crosshead Position for Specimen T5

The second test performed at an initial bolt torque of 27 N-m, specimen T6, achieved a maximum load of 376 kN, which was 4% less than specimen T5. The load-FRP strain relation for specimen T6 was similar to the load-FRP strain relation for the first test performed at an initial bolt torque of 27 N-m, as shown in Figure 5.14.

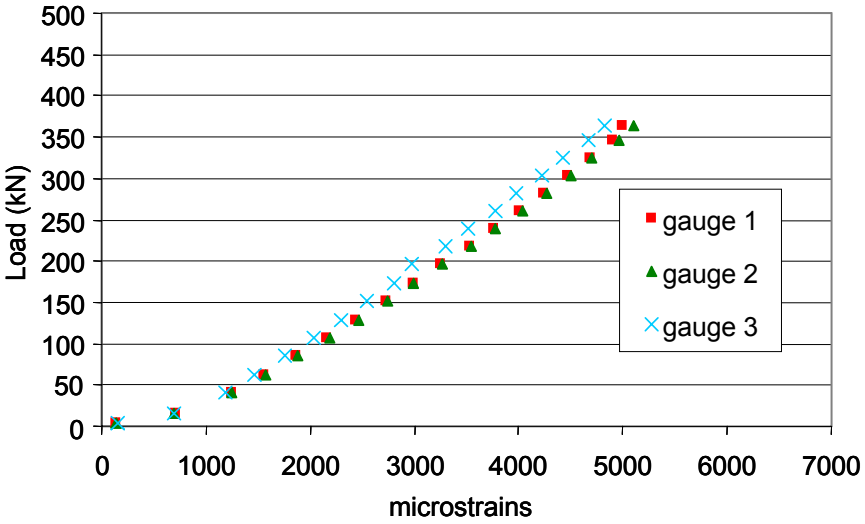

Figure 5.14 Load-Strain Relation for Specimen T6

Only three of the strain gauges survived the installation of specimen T6. The average slope of the load-strain relationship between 45 kN and 333 kN for specimen T6 was 84.7 N/microstrain. Specimen T6 exhibited a similar failure mode to the previous specimens, including slippage of the steel-FRP bond that resulted in shear plug failures of the reinforced glulam. Figure 5.15 shows the load-deformation response of specimen T6.

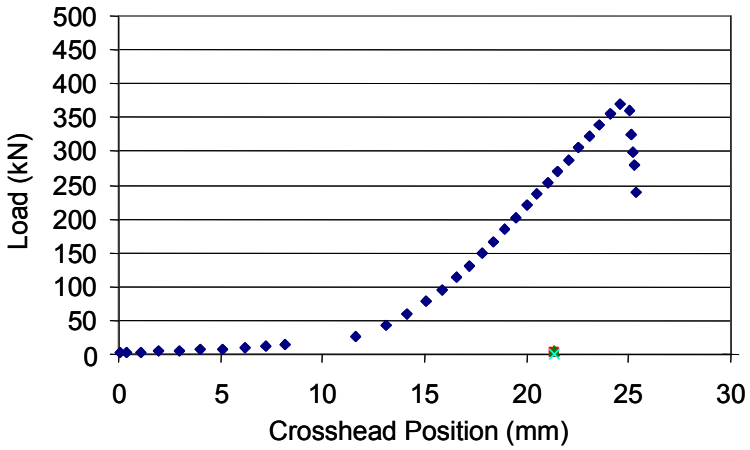

Figure 5.15 Load vs. Crosshead Position for Specimen T6

The average capacity for the specimens with 27 N-m of initial bolt torque was 383 kN, a 16% decrease from the average capacity of specimens T1 and T2, and a 10% decrease from the average capacity of specimens T3 and T4. The average stiffness of the connection, load-FRP strain slope evaluated between 45 kN and 333 kN, was 84.0 N/microstrain. More slippage of the steel-FRP bond

occurred than with the previous tests performed at higher bolt torques. This increased slippage resulted in a larger shear plug failure in the reinforced glulam. Peeling stresses likely played a larger role in the failure mode than in previous tests, which resulted in the lower load capacity for the specimen. However, with 27 N-m of initial bolt torque, the connection still maintained on average 1.6 times the 240 kN anticipated tensile load on the splice connection.

5.5 Durability Testing

An additional set of tests was performed on the splice connection to study the durability and delamination potential of the connection. These durability tests are important to qualify the behavior of the splice connection and glulam under adverse exterior environmental conditions. The test used to qualify the durability of the bonding of the steel to the FRP and the FRP to the steel was the ASTM D1101 delamination test, which was discussed in Section 3.

A total of three delamination specimens that included the bonded steel splice plate were tested. Additionally, three control specimens were tested without the steel splice plate. It was not possible to fabricate a 152mm long splice and cut it into two, 76mm long specimens due to the heating associated with cutting the steel. Therefore, 76mm long sections of reinforced rail were cut and a 76mm long piece of steel was bonded onto the reinforced glulam. The splice specimens which were tested for the ASTM D1101 were fabricated with the same adhesive and procedures as discussed earlier in this chapter.

The effects of the ASTM D1101 test are displayed in the Figure 5.16. All of the specimens exhibited no measurable delamination at either the steel-FRP bond or the wood-FRP bond, and therefore passed the ASTM D1101 test method A. For the control specimens, there were similar limited delaminations between the wood and FRP in the areas of gaps in the wooden glulam, similar to the specimens tested previously and discussed in Section 3.

This good performance is likely due to the thick steel-FRP epoxy bond and the FRP itself acting as a compliant layer between the steel and the wood, which alleviated the high shear stresses that would otherwise develop if the steel was bonded directly to the wood with a thin layer of adhesive. The extent to which the steel restrained hygrothermal movements is evident in Figure 5.17, which shows a close-up view of the corner of both a splice and a control specimen. Overall, the addition of steel to the reinforced hardwood glulam decreases the delamination of the FRP from the wood. There was also no delamination of the steel from the FRP in the test. The bonded steel splice connection passed the ASTM D1101 test.

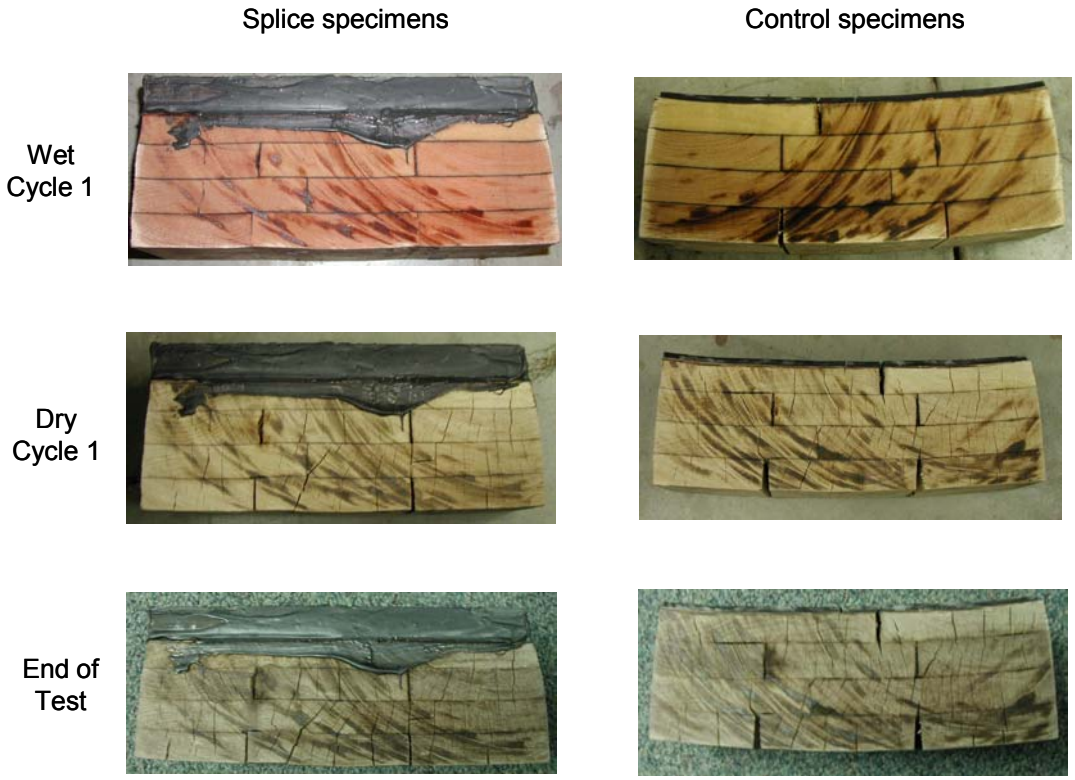

Figure 5.16 ASTM D1101 Specimens

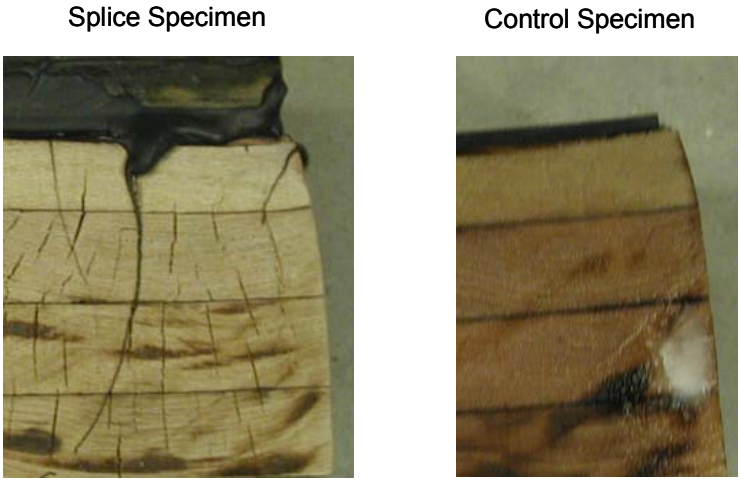

Figure 5.17 Close-up of Corner of ASTM D1101 Specimens

5.6 Summary

The testing of the rail splice connection showed that the splice connection has sufficient capacity for use in the reinforced guardrail, even with minimal bolt torque. The average capacity decreased by only 16% with a drop in bolt torque from 136 N-m to 27 N-m. We emphasize that an initial bolt torque of 27 ft-lbs corresponds to a very loose connection, and yet both of the tests performed at this torque level maintained a tensile capacity greater than 360 kN, which is 1.6 times the predicted demand on the splice connection. The bonded steel splice connection also passed the ASTM D1101 durability test and therefore the splice connection should be suitable for exterior exposure.

6. Combined Bending and Tension Testing

This section details a program designed to test the guardrail under combined bending and tension, which is necessary to evaluate the performance of the guardrail under vehicular impact. First, the development of a novel test fixture that produces controlled tension in the rail due to the shortening of the rail in flexure is presented. Second, the test setup and instrumentation are discussed. Finally, the results of the testing program are reported.

6.1 Design of the Bending-Tension Reaction Fixture

Producing bending simultaneously with tension in the guardrail can be accomplished in several different ways. The obvious solution would be to use two actuators, the first to apply a transverse load producing bending, and the second to apply direct tension. However, this approach would require complex actuator controls and mounts. The more practical alternative chosen here utilized the three-member truss supporting each end of the specimen shown in Figure 6.1.

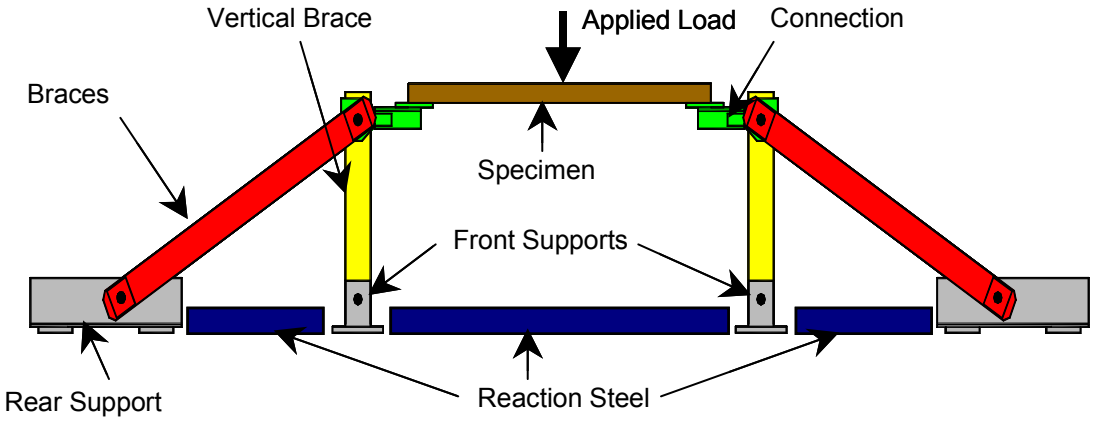

Figure 6.1 Combined Bending and Tension Reaction Fixture

As the projected horizontal dimension of the rail decreases due to flexure, the trusses act as springs, inducing tension in the rail. The challenge in this approach lies in analyzing the system appropriately and sizing the braces so that the desired tensile force is produced for a given applied transverse load. The idealization of the test set-up and critical dimensions are shown in Figure 6.2. The full span of the rail specimen and connection was 2.438m between the pins, and rail sections had a total length of 1.829m. The model considered the rail sections to be 1.676-m long, the distance between the centerlines of the splice connection. The centerline of the beam was also 29-mm above the centerline of the pins. The fixture was modeled as a beam with an applied force *P* at one end and pinned connection at the other end.

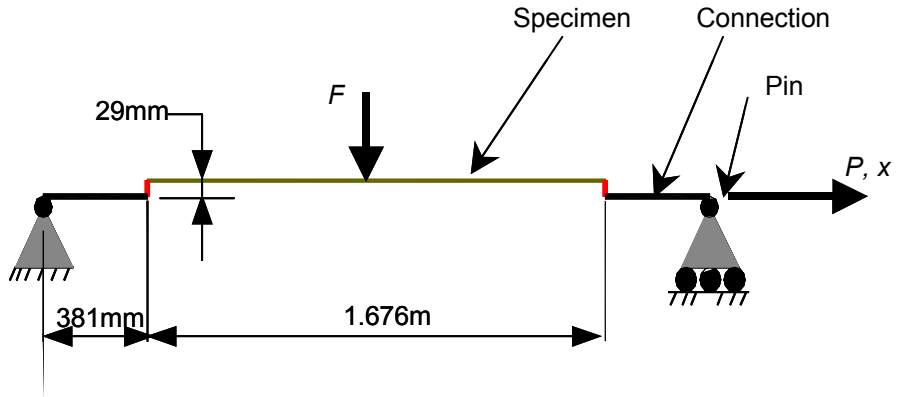

Figure 6.2 Idealization and Geometry of Combined Bending-Tension Test

The relationship between the applied transverse load, *F*, and the induced axial load, *P*, was quantified using small deformation, geometrically nonlinear structural analysis. The 2.438m span was idealized with three different 2-noded flexural elements. The 381mm distance from the pin centerline to the center of the rail splice connection was discretized with three-127mm elements having a moment of inertia and area corresponding to the connection detail. To capture the effect of the splice connection eccentricity, a 29-mm long vertical element with a very large moment of inertia and area was used from the centerline of the splice connection to the neutral axis of the beam. Finally, the 1.676m section of guardrail was modeled with 22 equal-length flexural elements having the same geometric and material properties determined from the flexural tests detailed in Section 3: an elastic modulus, *E*, of 10.3 GPa, a moment of inertia of 14×10^6 mm^4, and an area, *A*, of 23,000 mm^2.

The shortening of the rail section under flexure, Δ, was computed using Equation 6.1

$$\Delta = -\frac{P \cdot L}{A \cdot E} + \int_0^L \frac{1}{2} \cdot \left(\frac{dv}{dx} \right)^2 \cdot dx \qquad 6.1$$

In Equation 6.1, v is the transverse (flexural) displacement of the rail, and x is measured in the longitudinal direction. The first term in Equation 6.1 represents the axial lengthening of the rail due to P, which is relatively small, and the integral approximates the length of the rail specimen projected onto its longitudinal axis; the sum of these two quantities is the shortening of the rail. The development of Equation 6.1 can be found in texts on advanced or nonlinear structural analysis such as McGuire et al. (2000).

In the idealization of the test setup, the support trusses are treated as springs, and thus the axial force P is linearly dependent on the shortening of the rail section due to flexure. To account for this effect, the solution algorithm given in Algorithm 6.1 was developed and implemented. In Algorithm 6.1, k represents the net horizontal stiffness of each supporting truss, and thus $P = ½k\Delta$ since each truss must deform equally and develop the force P to maintain equilibrium.

set *tolerance* = 0.001
while *error* < *tolerance*
    $P_{old} = P_{new}$
    analyze structure under P_{new} and F
    compute Δ
    $P_{new} = ½\ k\ \Delta$
    error = abs($P_{new} - P_{old}$)/ P_{old}
end

Algorithm 6.1: Solution Strategy

Algorithm 6.1 and the required geometrically nonlinear structural analysis program were implemented using the scientific and engineering computation package Matlab. The target value for the sizing of the braces was a tensile force of P = 178 kN induced in the rail due to a transverse load F = 58 kN. These target values were based on preliminary analyses using Barrier VII, similar to those discussed in Section 2. However, these preliminary Barrier VII models used estimated material properties and a preliminary rail cross-section. Further, the original structural model and implementation of Algorithm 6.1 had several errors and did not properly account for the eccentricity of the splice connection and the stiffness of the braces. The net result of these approximations and errors was that the test fixture as designed and constructed had braces with a net horizontal stiffness, k, of 259 kN/mm, which was lower than desired value based on the updated Barrier VII analyses reported in Section 2. However, the results of the testing program presented later in this section show that the measured response of the test rig compares quite well with the predictions of the model as detailed here, and the test rig did allow the development of a tensile force P significantly in excess of 240 kN, the maximum expected force in the

rail section, at a reasonable value of *F* for all specimens tested. Detailed drawings of the supporting truss are given in the Appendix of this report.

6.2 Bending-Tension Test Setup

6.2.1 Fabrication of Combined Bending and Tension Specimens

In order to develop significant tension in the system, it is necessary to hold tight tolerances during fabrication of the rail splice connections and minimize slippage in the connections during the tests. In order to minimize the misalignment of the specimens and gaps in the system, a special fixture was used to align the steel splice plates while they were bonded to the rail. The bolt holes were the precise size of the bolts, and the overall length of the specimen was 1.829m. The length of the glulam was 1.822m to allow the specimen to fit into the fixture. A 152mm by 254mm by 13mm thick steel plate was bonded to the FRP-reinforced glulam for the bolted splice connection using the same protocols discussed in section 3.

The specimens were fabricated by first grit blasting the steel, then placing 162 g of epoxy on the bonded steel connection plates, as described previously in Section 5, and placing the bonded steel connection plates into the fixture. Next, the reinforced glulam was placed on top of the epoxy-covered bonded steel connection plates in the fixture. Then approximately 21 kPa of pressure was applied to the reinforced glulam as it was moved to remove air from the bond line and squeeze out excess epoxy. Finally, the reinforced glulam was aligned on the fixture and left to cure for three days. There was excess epoxy squeezed out on all of the specimens fabricated, and as described later in this section, none of the specimens failed due to poor bond quality. The alignment fixture with a glulam and bonded steel splice plates in place is shown in Figure 6.3.

Figure 6.3 Alignment Fixture

6.2.2 Combined Bending and Tension Test Setup

The test setup for the combined bending-tension tests was the reaction fixture that was designed to apply tension from the shortening as previously discussed in this Section. The reaction frame is shown schematically in Figure 6.1 and detailed dimensions of the reaction fixture can be found in Appendix 1. Alexander's Welding and Machine, Inc. of Greenfield, Maine, fabricated the test fixture.

The rear supports were bolted to the reaction floor using two-36mm diameter Dywidag bars, and the front supports were bolted to the reaction floor using 25mm diameter threaded rods. The reaction frame was held together with 51mm diameter pins of 4140 steel having a yield strength of 968 MPa. Three pieces of C12X20.9 channel were bolted to the reaction floor to make the system self-reacting. The center section of channel was bolted to the floor with two 25mm diameter threaded rods, at one third of the length from the ends. Each end piece of channel was connected to the reaction floor with one 25mm diameter threaded rod at its center. There were gaps between the ends of all three of the reaction steel channels and the truss supports. Different thickness shims were hammered into these gaps immediately prior to starting each test to ensure that all of the gaps in the system were removed and that the entire truss was self-reacting in the horizontal direction.

The specimens were loaded with a 500 kN actuator mounted beneath the floor. The actuator was connected to a reaction frame on which a 250 kN load cell was mounted with a radiused wooded load head attached to the load cell. The load head rested on a 25mm thick rubber pad placed on the beam to distribute the load. The complete setup is shown in Figure 6.4:

Figure 6.4 Bending-Tension Test Rig

6.2.3 Instrumentation and Data Acquisition

The instrumentation used to acquire the data for the combined bending-tension test was similar to that used in the pure bending test. The load and position were acquired from the Instron controller. As with the bending tests detailed in Section 3, the displacement that was output by the Instron controller included not only the displacement of the beam, but also the compression of the rubber pad and the load head, which was significant at high loads. The compression of the load head and rubber pads was subtracted from the load head displacement using the same method detailed in Section 3.

Four Measurements Group CEA-06-125UW-350 strain gauges were bonded to the FRP with MBond –200 epoxy. Two pairs of gauges were used: one at the center of the beam and one at ½ of the length between the center of the beam and the end of the bonded steel connection plate, with each gage located 63mm from the specimen edge.

Eight strain gauges were used on the diagonal braces of the reaction frame, two gauges on each of the four braces. Each gauge was centered longitudinally and vertically on the braces, with one on each side of each brace. The strain measured in the steel braces was used to calculate the tension applied to the guardrail specimen using the nominal modulus of elasticity of steel and the cross-sectional area of each brace.

6.3 Bending-Tension Test Results

A total of three combined bending-tension tests were performed in displacement control with a displacement rate of 13mm per minute. All connection bolts were torqued immediately prior to loading to 136 N-m to reduce slippage in the connection. In all three tests the wood exhibited a tensile failure at between 80 and 95 kN of applied transverse load, but the specimens continued to gain significant transverse load and tension after the wood tensile failure.

6.3.1 Specimen BT1

Specimen BT1 was loaded twice due to initial concerns regarding the safety of the test fixture. The fixture was originally designed to withstand a maximum applied transverse load of 130 kN and 260 kN of axial load. However, the specimen did not fail under these loads. Thus, for safety reasons, the first loading was halted when the applied transverse load reached 118 kN at an axial load of 276 kN. The specimen did encounter a tensile lamination failure during the first loading of the specimen at approximately 91 kN of applied transverse load. The fixture capacity was then reevaluated using less conservative assumptions, and it was deemed safe for the fixture to sustain a transverse load of 178 kN and an axial load of 489 kN. Several days later, specimen BT1 was retested. During the second loading

the specimen exhibited a reduced stiffness at low loads due to the previous partial failure of the wood in tension. The load-displacement relation for specimen BT1 is shown in Figure 6.5.

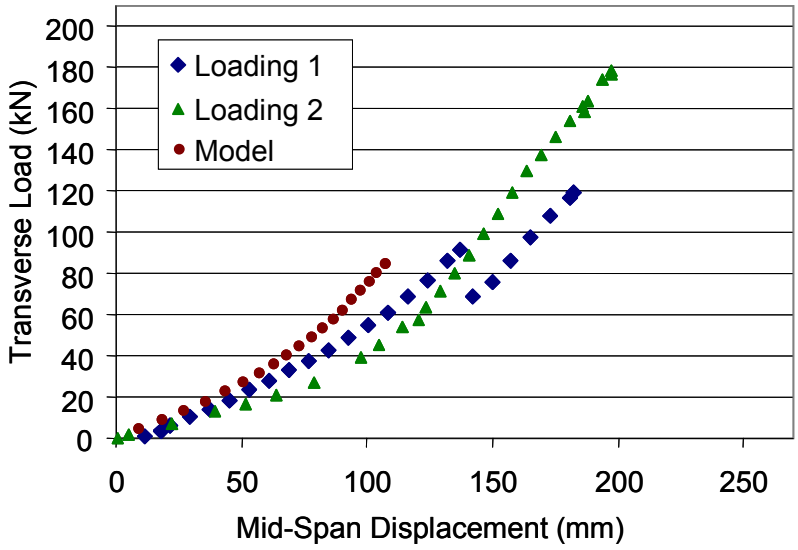

Figure 6.5 Specimen BT1 Load-Displacement

The first loading continues to the point at which the wood tensile failure occured in the glulam at 91 kN of transverse load. The failure of the wood tensile lamination occurred at a finger joint located approximately 110mm from mid-span, and caused delamination of the FRP. However, this delamination was not a failure of the glulam-FRP bond, since several layers of FRP were still attached to the glulam and FPL-1 epoxy. The load-displacement curve then drops sharply and continues until an applied transverse load of 119 kN, at which point the first loading was halted.

The second loading exhibits a reduced initial stiffness due to the failed wood tension lamination, and the load-displacement response is relatively smooth until the maximum transverse load of 179 kN. The model predictions are also shown in Figure 6.5, and agree reasonably well with the observed response during the first loading sequence. The effect of tension stiffening due to the restraint of the supports is clearly evident in both the measured and predicted response.

As the load approached the maximum, the FRP at the locations of the bolt holes broke free of the steel-FRP bond and delaminated from the rest of the FRP. When the second loading sequence was stopped, the position of the actuator was held constant. The specimen continued to carry load, but after 96 seconds, the steel-FRP bond crept significantly, which led to a rapid drop in the transverse load. We note that this creep of the steel-FRP bond would not reduce the capacity of a guardrail during a vehicular impact due to the very short duration of the loads induced by vehicular impact.

The applied transverse load to induced axial load relation for specimen BT1 is shown in Figure 6.6. The maximum axial load induced during the second loading of the beams was 435 kN. The relationship between applied transverse load and axial tension in the rail is nonlinear due to the tension restraint provided by the support trusses. The model-predicted and measured responses are in good agreement.

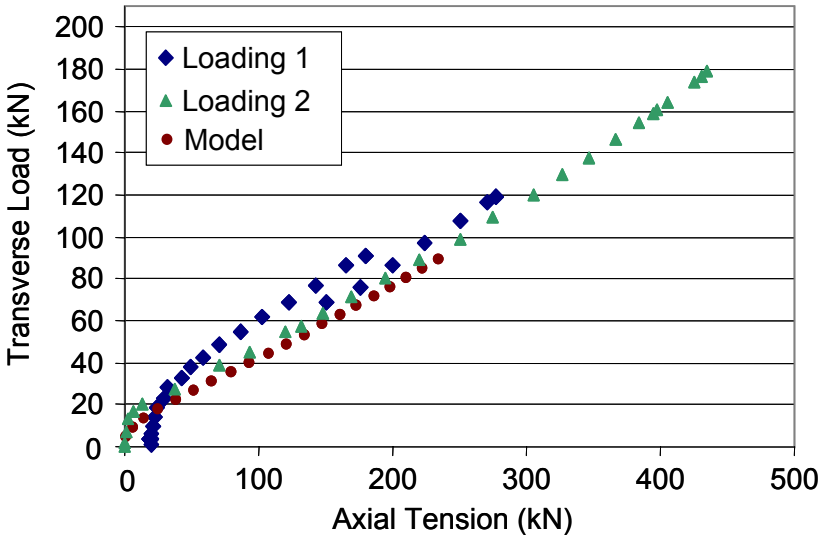

Figure 6.6 Specimen BT1 Transverse Load vs. Axial Tension

The relationship between applied transverse load and the strains measured in the FRP is shown in Figure 6.7. The measured strains show a highly nonlinear response with applied transverse load. Based on the published properties of the Gordon Composites GC-67-UB FRP under tensile loads and the measured FRP strains, the maximum stress sustained by the FRP was 595 MPa, 62% of its published ultimate capacity. We note that this computed stress is an extreme fiber stress due to both axial tension and curvature of the FRP.

In summary, despite the loss of bond between the glulam and the FRP, specimen BT1 attained a peak applied transverse load of 179 kN, with an induced tensile load of 435 kN. Both the applied transverse load and induced axial load were significantly higher than the expected capacity. Further, specimen BT1 did not fail under these loads.

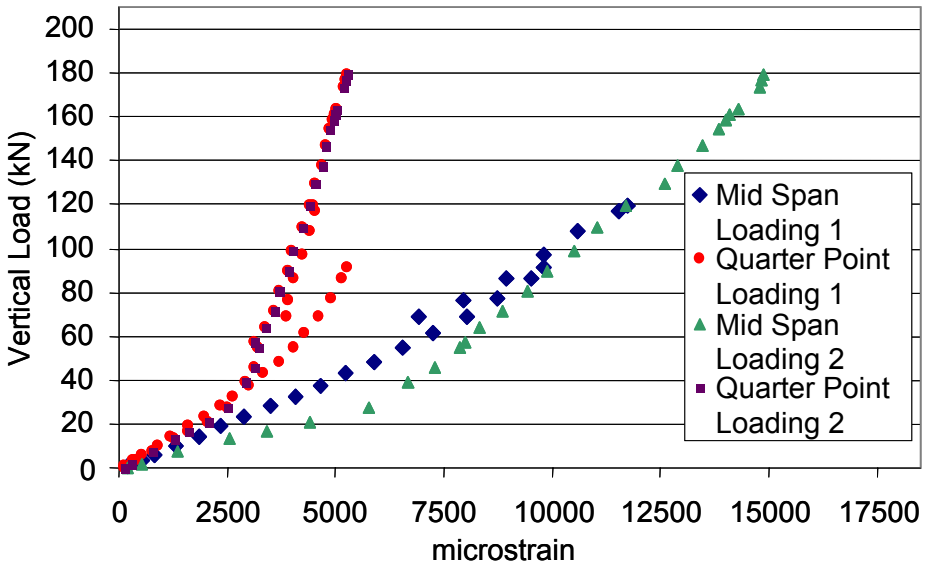

Figure 6.7 Specimen BT1 FRP Strains

6.3.2 Specimen BT2

The second combined bending-tension test was performed on specimen BT2. This specimen was shimmed and initially loaded until the applied transverse load was 44 kN. Significant axial loads had not yet developed at this load, so the load was removed and larger shims were added to the system to remove the gaps. The specimen was then reloaded, and significant axial loads were developed. The load-displacement relationship for specimen BT2 is shown in Figure 6.8. The applied transverse load to displacement relationship for specimen BT2 is not as smooth as specimen BT1, however the magnitudes of the applied load and observed displacements are similar to those of specimen BT1. The wood experienced a tensile failure at an applied transverse load of 83 kN. Unlike specimen BT1, the FRP did not delaminate from the wood. The agreement between the model predictions and the observed response is quite good, and the tension stiffening effect is clear from the measured response and model predictions.

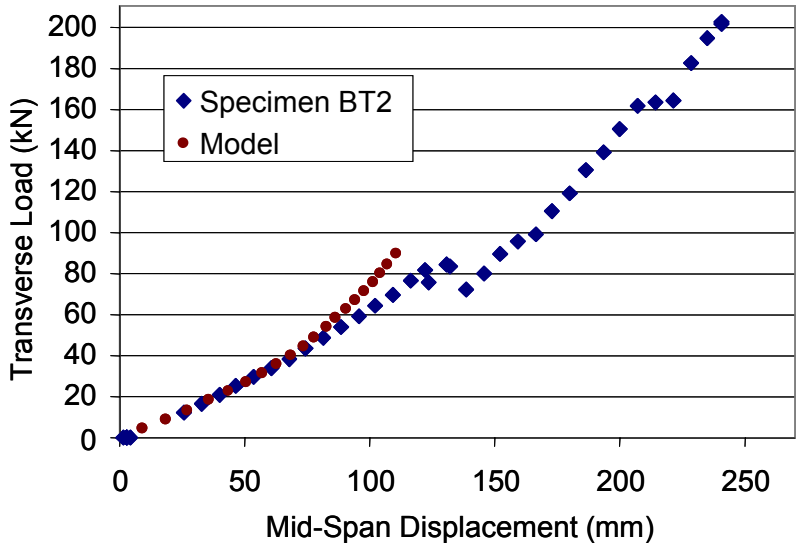

Figure 6.8 Specimen BT2 Load-Displacement

The relationship between the applied transverse load and the induced axial load is shown in Figure 6.9. The maximum applied transverse load was 202 kN, corresponding to a maximum induced axial load of 461 kN. The model-predicted tensile forces agree well with the observed response.

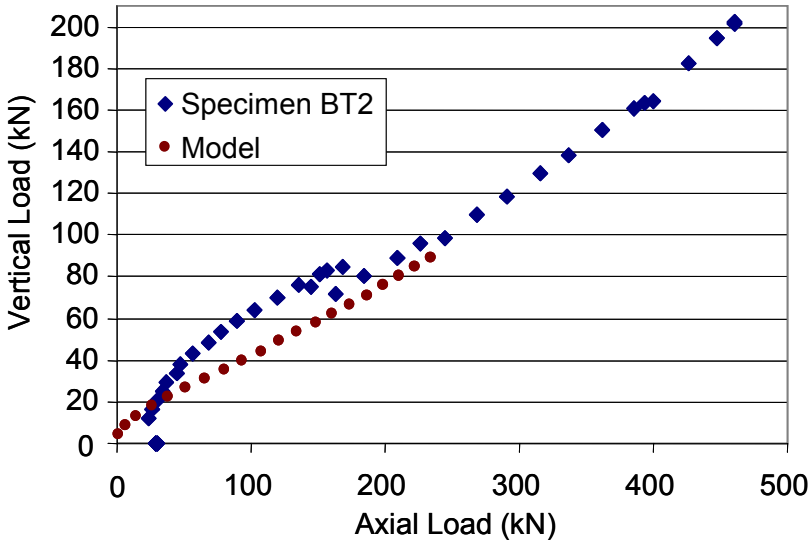

Figure 6.9 Specimen BT2 Transverse Load vs. Axial Tension

The relationship between applied transverse load and FRP strain for specimen BT2 was similar to that observed for specimen BT1 as shown in Figure 6.10. The strains displayed are the average of each pair of strain gauges until one of the gauges is damaged, then the functioning gauge values are reported. Based on the published value for the elastic modulus of the Gordon Composites GC-67-UB FRP in the

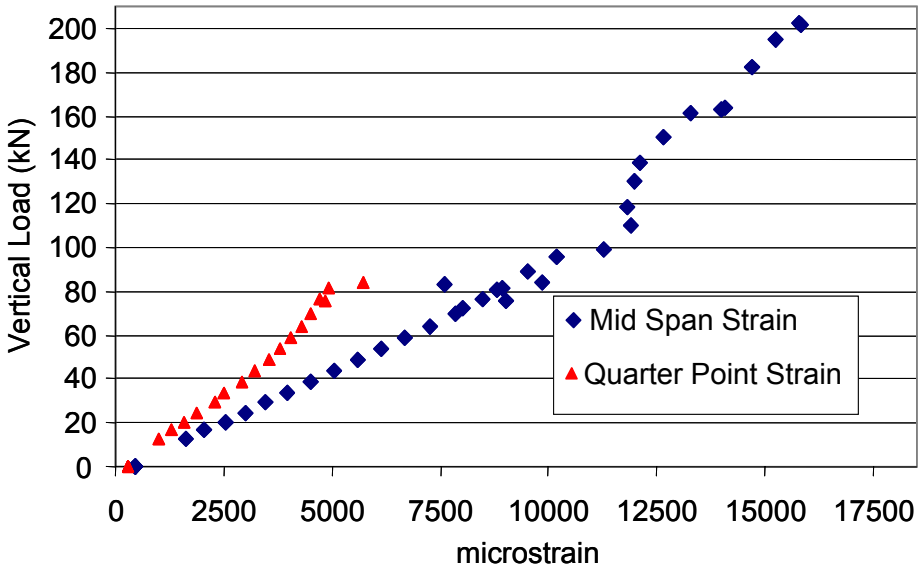

Figure 6.10 Specimen BT2 FRP Strains

fiber direction under tensile loads, the maximum stress attained by the FRP was 632 MPa, or 67% of its published ultimate capacity. The applied loads exceeded the capacity of the test fixture, and the connections yielded in flexure. This created a slight upward tilt in the bolted connection as well as elongation of the fixture, which required additional shimming for the final test.

6.3.3 Specimen BT3

The third combined bending-tension test was performed on specimen BT3. Due to the yielding in the bolted connection that occurred during the testing of specimen BT2, additional shimming was needed in the system to remove gaps prior to loading specimen BT3. The effects of the yielding on the connection can be seen in Figure 6.11.

Figure 6.11 Yielded Connection

The load-displacement relation for specimen BT3 is shown in Figure 6.12. Specimen BT3 exhibited two wood tensile failures: the first tensile failure occurred at an applied transverse load of 94.5 kN, and the second tensile failure in the wood occurred at 102 kN of applied load. Aside from the double tensile failure the results for specimen BT3 are similar to those of specimens BT1 and BT2.

The maximum applied transverse load for specimen BT3 was 179 kN, which induced an axial load of 422 kN. The transverse load to axial load relation is shown in Figure 6.13. Due to the inclined connection, specimen BT3 exhibited some arching action at low applied transverse loads. The effects of the arching on the induced axial load is evident in Figure 6.13, where the load decreased slightly from the initial load due to shimming, and then rose again once the beam had overcome the arching action. With the exception of this initial response, the relationship between applied transverse load and induced axial load was similar to those observed in previous tests.

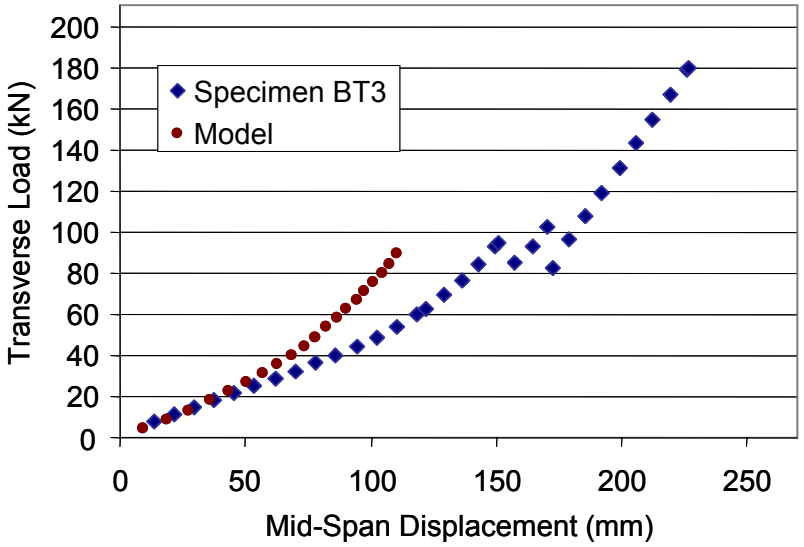

Figure 6.12 Specimen BT3 Load-Displacement

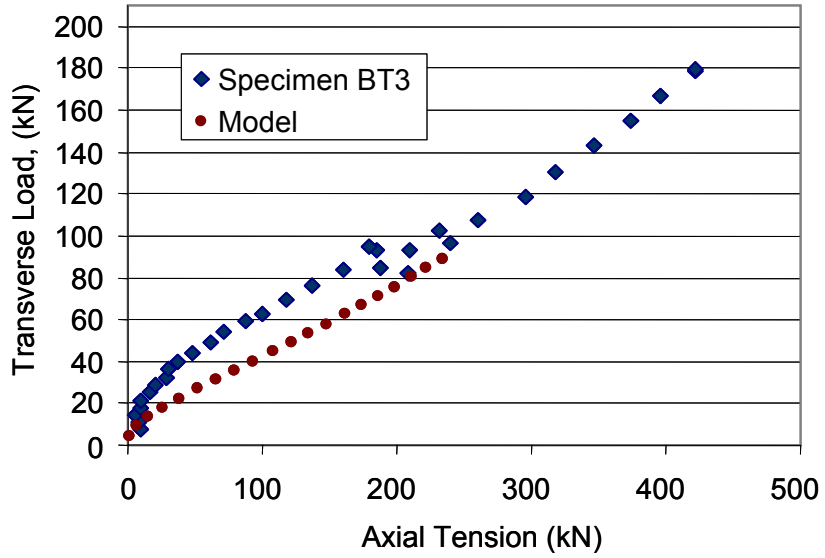

Figure 6.13 Specimen BT3 Transverse Load vs. Axial Tension

The load strain relation is presented in Figure 6.14. Based on the published value of the average elastic modulus of the Gordon Composites GC-67-UB FRP in the fiber direction and under tensile loads the maximum stress attained by the FRP was 719 MPa, 76% of its published ultimate capacity.

Near the end of the test, the load head moved laterally about 25mm off the center of the specimen. At the conclusion of the test, the loading frame was visibly tilted. No explanation was reached for the movement of the load head or the angle of the load frame. A 6mm-wide strip of FRP delaminated and detached from one outside edge of the specimen. This may have resulted from torsion induced in the rail by the lateral shift in load head position. Despite the torsion due to the lateral shift of the load head,

the response of specimen BT3 was similar to that of BT1 and BT2, and the specimen did not fail under the applied loads.

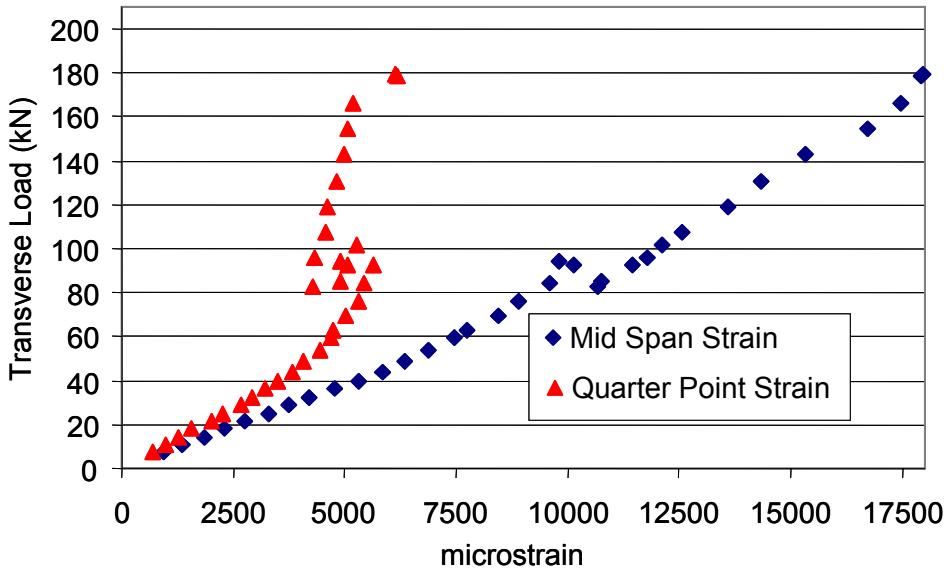

Figure 6.14 Specimen BT3 FRP Strains

6.4 Summary and Conclusions

Three successful combined bending and tension tests were performed. Due to the limited capacity of the bending-tension test frame and the larger-than expected capacities of the specimens, none of the specimens were tested to failure, and all the specimens were carrying the peak observed loads when the tests were halted. Specimen BT1 did fail in creep under constant displacement after the static test was halted. The critical results of the three tests are summarized in Table 6.1.

Table 6.1 Summary of Bending-Tension Test Results

Specimen	Load at Wood Tension Failure (kN)	Induced Axial Force at 170 kN Load	Maximum Applied Load (kN)	Maximum Mid-Span Deft. (mm)
BT1	91.2	411	179	197
BT2	83.0	418	202	241
BT3	94.5	404	179	226

The results were very consistent between tests. The average maximum applied transverse load and induced tension far exceed the anticipated loads on guardrails under impact as discussed in Section 2. Further, the models of Section 2 predict a maximum deflection of the rail between two posts of 140mm, and all of the specimens sustained a peak deflection of more than 1.4 times this value. These unique

bending-tension tests indicate that the rail should have sufficient structural capacity to survive a vehicular impact.

7. Summary and Conclusions

7.1 Summary

A guardrail has been developed that consists of a 254mm deep by 76mm thick reinforced hardwood glulam reinforced on one face with 3.5-mm of unidirectional E-glass FRP. The properties of the reinforced glulam design were evaluated using transformed section analysis, and the response of the guardrail system under vehicular impact was modeled with Barrier VII (Powell, 1973). The analyses indicate that the barrier deflections and vehicle accelerations are comparable with those of a standard steel W-beam guardrail system, and that tensile forces as high as 240 kN are present at the splice connections of the rail during a TL-3 crash test.

In order to carry the large tensile forces between the adjacent rails, a specialized field-bolted splice connection was developed. This splice connection relies on a steel plate bonded to the E-glass reinforcement. This bond allows the tensile force to be transferred into the FRP through shear in the steel-FRP bond.

The reinforced glulam both with and without the splice plate was tested for durability under exterior environmental conditions using the ASTM D1101 test method. Through all of the delamination testing there was minimal quantifiable delamination. Both the reinforced hardwood glulam and the splice connection passed the ASTM D1101 test and appear to be suitable for exterior use.

Two three-point bending tests were performed on the reinforced guardrail sections. The specimens tested in bending both behaved similarly and demonstrated nonlinear load-displacement response due to flexural compressive yielding of the wood. The average failure moment for the bending tests was 37 kN-m.

Six splice connections were eccentrically loaded in tension to simulated tensile forces in a rail splice connection during vehicular impact. The torque load in the bolts played a role in the behavior of the tensile specimens. Two specimens each were tested at the initial bolt torques of 136-N-m, 54 N-m, and 27 N-m. The specimens tested at 136 N-m of initial bolt torque had an average capacity of 463 kN, the specimens tested at 54 N-m of initial bolt torque had an average capacity of 427 kN, and the specimens tested at 27 N-m of initial bolt torque had an average capacity of 383 kN, all of which are greater than the expected tension load of 240 kN. We note that a bolt torque of 27 kN is very low, and corresponds to a loss of 80% relative to an initial torque of 136 N-m.

In addition to tension, it was necessary to test the reinforced glulam guardrail and splice connection under combined bending and tension. To accomplish this, a specialized fixture was designed

that induced tension in the rail due to shortening of the rail under flexure. The fixture was a single panel truss that was bolted to the reaction floor and pin-connected to the splice connection. The truss was rationally designed using 2nd-order geometrically nonlinear structural analysis techniques, which also allowed the prediction of specimen response during testing. Three specimens were tested under combined bending and tension, and encountered tensile failures in the wooden glulam at approximately half the maximum applied transverse load. However, the FRP reinforcing behaved as a tension ribbon, providing additional capacity. The average peak transverse load that was applied was 187 kN, and the average peak induced tension was 439 kN. None of the specimens failed and all three specimens were carrying the applied loads at the conclusion of the test. The specimens demonstrated capacities well in excess of the expected demands on a guardrail during a vehicular impact.

7.2 Conclusions and Recommendations

Testing and modeling indicates that the 76-mm deep reinforced hardwood glulam guardrail as designed is structurally sound for use in a guardrail system. Models of the reinforced glulam guardrail section indicate that it would perform similarly to a standard W-beam guardrail with regard to anticipated deflections and vehicular decelerations. The cost of the installed reinforced hardwood glulam guardrail excluding posts and blockouts is estimated at $118/m. We note that the installed cost of a steel-backed timber guardrail system in Maine is approximately approximately $150/m (MDOT 2002), which implies that the FRP-reinforced timber guardrail should be cost-competitive if posts and blockouts can be installed for approximately $32/m.

However, further work is required before the system is ready for field implementation. Preservative treatments and their effect on the wood-FRP bond need to be studied. Also, it may be beneficial to investigate alternate lamination schemes, such as horizontal stacked laminations. These methods are less expensive ways to obtain the 76mm rail cross-section than the brickwork layup used in this study. A critical parameter that would need to be evaluated is the quality of the wood-FRP bond, which could be adversely affected by the use of horizontally stacked laminations. It is recommended that crash testing of the reinforced hardwood glulam guardrail be pursued once these remaining issues are resolved.

The excess capacity demonstrated in the tension and bending-tension tests indicate that it may be possible to reduce the cross-sectional dimensions, splice connection length, and number of bolts in the splice connection. However, the sizes of the rail section and the connection as designed and tested are quite reasonable. Further, given the uncertainty inherent in the estimation of guardrail response, additional modeling and testing are strongly recommended before the capacity of any element of the guardrail is

reduced. Finally, it is also possible that the splice connection developed in this study has applications for heavy timber tension connections, which could be a fruitful area of future research and development.

8. References

AISC (2002). *Manual of Steel Construction, Load and Resistance Factor Design*, Chicago: American Institute of Steel Construction Inc.

ASTM (2002a). *Standard Test Method for Integrity of Adhesive Joints in Structural Laminated Wood Products for Exterior Use*. ASTM D1101 Baltimore, MD: American Society for Testing and Materials.

ASTM (2002b). *Standard Specifications for Adhesives for Structural Laminated Wood Products for Use Under Exterior (Wet Use) Exposure Conditions*. ASTM D2559, Baltimore, MD: American Society for Testing and Materials.

Boone, M. J., (2002). *Mechanical Testing of Epoxy Adhesives for Naval Applications,* Master of Science Thesis, University of Maine.

Calcote, R. and Kimball, C.E. (1978). Properties of Guardrail Posts for Various Soil Types. *Transportation Research Record*. *No. 679*, pp. 22-25. Transportation Research Board, Washington, D.C.

Chen, C.-J. (1998). Mechanical Performance of Fiberglass Reinforced Timber Joints. In J. Natterer & J.-L. Sandoz (Eds.) *Proceedings of the 5th World Conference on Timber Engineering* (pp. 500-507). Montreux, Switzerland.

Dagher, H. J., and Lindyberg, R. (2003). Development of the AASHTO Specifications for FRP-Reinforced Glulam Beams. *Presented at the 82nd Annual Meeting of the Transportation Research Board.* January 12-16, 2003, Washington, D.C. (CD-ROM)

Forest Products Lab, (1999). *Wood Handbook: Wood as an Engineering Material*, Madison, WI: Forest Products Lab.

Gordon Composites, Inc. (2001). http://www.gordoncomposites.com/UB_Specs.htm

Lopez-Anido, R., Gardner, D. J., and Hensley, J. L., (2001). Adhesive Bonding of Eastern Hemlock Glulam Panels with E-glass/Vinyl Ester Reinforcement. *Forest Products Journal,* 50, 43-47.

MDOT (2002). http://www.state.me.us/mdot-old/project/design/bt920900.htm

McGuire, W., Gallagher, R. H., and Ziemian, R.D. (2000). *Matrix Structural Analysis, Second Edition.* New York: John Wiley & Sons, Inc.

NCHRP (1993). *NCHRP Report 350: Recommended Procedures for the Safety Performance Evaluation of Highway Features*. Transportation Research Board. National Research Council. Washington, D.C.

Ogershock, D. (2002). *2002 National Construction Cost Estimator*. Carlsbad, CA: Craftsman Book Company.

Patzner, G.S., Plaxico, C. A., and Ray, M. H. (1998). Effect of Post and Soil Strength on the Performance of a Guardrail Terminal. H. Murakami & J. E. Luco (Eds.) *Proceedings of the 12th Engineering Mechanics Conference* (pp. 170-173). La Jolla, California.

Powell, G. H. (1973). *Barrier VII: A Computer Program for Evaluation of Automobile Barrier Systems* (FWHA Report Number FWHA-RD-73-51). Springfield, VA: U.S. Department of Commerce, National Technical Information Service.

Rosson, B. T., Bierman, M. G., and Rohde, J. R. (1997). Assessment of Guardrail-Strengthening Techniques. *Transportation Research Record. No. 1528,* pp. 69-77. Transportation Research Board, Washington, D.C.

Soltis, L.A., Ross, R. J., and Windorski, D. F. (1998). Fiberglass-Reinforced Bolted Wood Connections. *Forest Product Journal*, 48 (9), 63-67.

Ritter, M.A. (1992). *Timber Bridges: Design, Construction, Inspection and Maintenance*. USDA Forest Service, Washington, D.C., Report No. EM 7700-8.

Tuan, C. Y., Post, E. R., Ataullah, S., and Brewer, J.O. (1989). Development of Kansas Guardrail to Bridgerail Transition Designs Using BARRIER VII. *Transportation Research Record, No. 1233*, pp. 145-154. Transportation Research Board, Washington, D.C.

9. Appendix

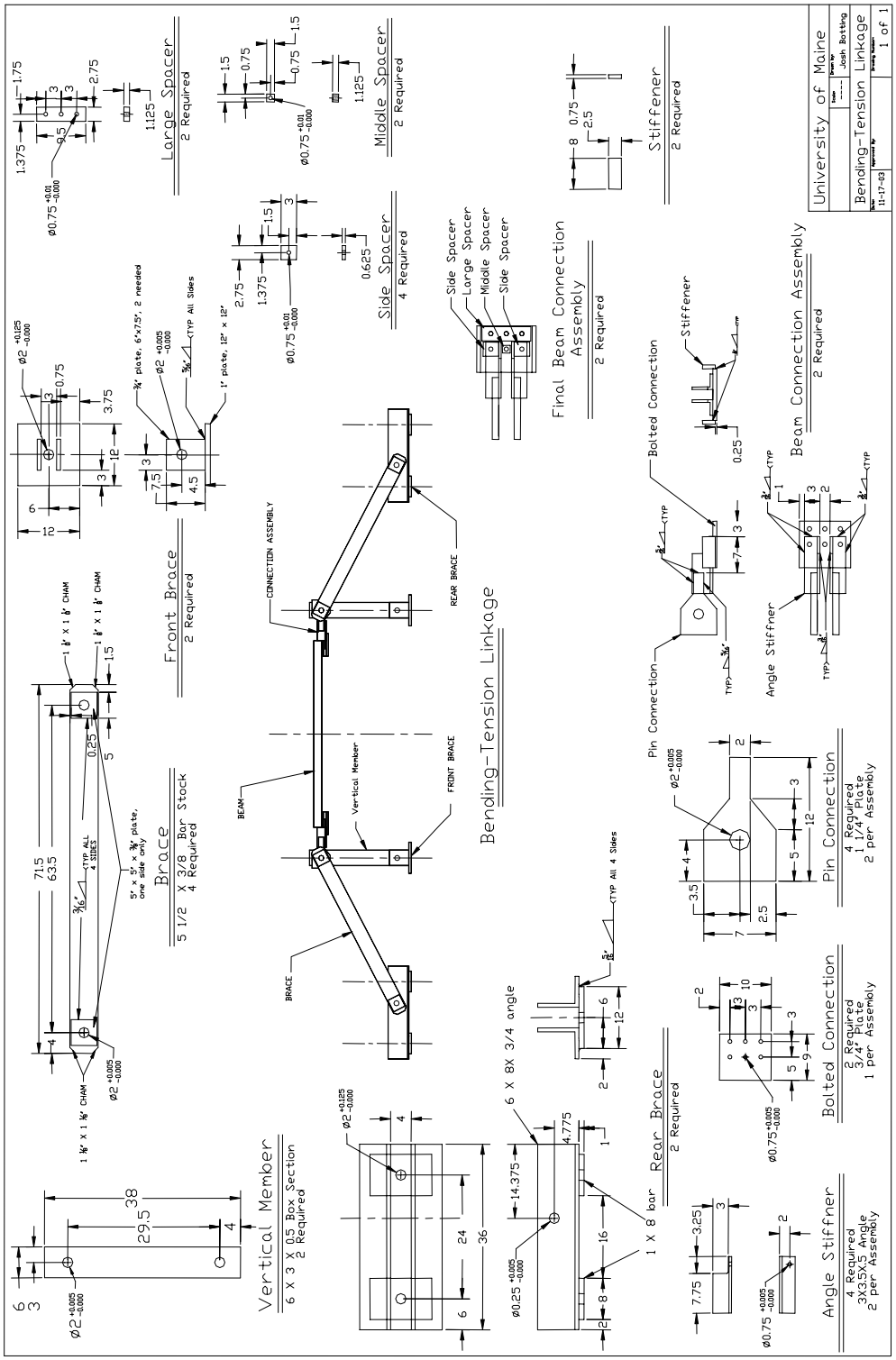

Figure A1 Details of Truss Supports for Combined Bending-Tension Tests